The study of the dynamic response of slender structures due to downburst outflows through full-scale monitoring

Mekdes Tadesse Mengistu

Department of Civil, Chemical and Environmental Engineering
University of Genova

This dissertation is submitted for the degree of
Doctor of Philosophy

Polytechnic School

August 2023

THE STUDY OF THE DYNAMIC RESPONSE OF SLENDER STRUCTURES DUE TO DOWNBURST OUTFLOWS THROUGH FULL-SCALE MONITORING

BY

MEKDES TADESSE MENGISTU

Dissertation discussed in partial fulfillment of

the requirements for the Degree of

DOCTOR OF PHILOSOPHY

Department of Civil, Chemical and Environmental Engineering,

curriculum in Structural and Geotechnical Engineering,

University of Genoa, Italy

August, 2023

Adviser:
Prof. Maria Pia Repetto - Civil, Chemical and Environmental Engineering, University of Genova

External Reviewers:
Prof. Teng Wu - Civil, Structural and Environmental Engineering, University at Buffalo
Prof. Amal Elawady - Civil and Environmental Engineering, Florida International University

Examination Committee:
Prof. Paolo Bazzurro - Scuola Universitaria Superiore IUSS di Pavia
Prof. Federico Perotti - Politecnico di Milano
Prof. Domenico Gallipoli - Universita degli studi di Genova

Ph.D. program in Civil, Chemical and Environmental Engineering

Curriculum in Structural and Geotechnical Engineering

Cycle XXXV

This thesis is dedicated to my mother Etenesh Gezahegn.

"All that I am, or ever hope to be, I owe to my angel mother."
Abraham Lincoln

Declaration

I hereby declare that except where specific reference is made to the work of others, the contents of this dissertation are original and have not been submitted in whole or in part for consideration for any other degree or qualification in this, or any other university. This dissertation is my own work and contains nothing which is the outcome of work done in collaboration with others, except as specified in the text and Acknowledgements.

Chapter 3 of this dissertation has been published in the Journal of Wind Engineering and Industrial Aerodynamics with the title *"Wind and structural response monitoring of a lighting pole for the study of downburst effects on Structures"*

Chapter 4 of this dissertation has been submitted to the Journal of Wind Engineering and Industrial Aerodynamics with the title *"Dynamic response of a slender structure to thunderstorm outflow excitation through numerical analysis and full-scale monitoring"*

Mekdes Tadesse Mengistu
August 2023

Acknowledgements

First and foremost, I am indebted to my supervisor, Prof. Maria Pia Repetto, for her exceptional guidance, unwavering support, and kindness. From the moment we met, she has been a source of immense encouragement and has provided valuable mentorship. I am truly grateful for the research opportunities, collaborations, and dissemination platforms she provided, which have been instrumental to my growth as a researcher.

I would also like to extend my heartfelt appreciation to the late Prof. Giovanni Solari and the entire GS-WinDyn research group for teaching me the basics of wind engineering and swiftly integrating me into their esteemed group. To Prof. Federica Tubino and Prof. Luisa C. Pagnini, I express my sincere thanks for their valuable comments and insightful questions during my periodic evaluations, which have significantly improved the quality and depth of my research. I am particularly grateful to Prof. Federica Tubino for her support whenever I sought assistance in understanding the intricacies of random dynamics.

I am sincerely thankful to my colleague Andrea Orlando for introducing me to the full-scale monitoring system, providing me with his wind tunnel experiment results, and tirelessly answering my countless queries. Furthermore, I extend my gratitude to Xiao Li for introducing me to some of the operational modal analysis techniques. I would like to acknowledge the stimulating and enthusiastic discussions I have had with my colleagues Stefano Brusco and Luca Roncallo. Their valuable insights and perspectives have broadened my understanding and enriched my study. I extend my heartfelt appreciation to all my colleagues at DICCA. The cherished memories we have shared during our time together will forever hold a special place in my heart. To my friends from my home country and the amazing friends I have made in the beautiful city of Genova, I am grateful for your moral support and the joyous moments we have experienced together.

Last but certainly not least, I would like to express my deepest gratitude to my family. Their unwavering support, love, and encouragement have been the foundation upon which I have built my academic achievements.

Abstract

The wind-excited response of structures has been extensively researched in the past many years and as a result, proper approaches and testing procedures have been proposed to avoid undesirable vibration and failure of structures due to wind. However, these researches and approaches are addressed to synoptic winds, which are large-scale phenomena covering thousands of kilometers and lasting up to a few days. The wind speed time history during these events is characterized by a constant mean wind speed averaged over 10 minutes to 1 hour and a zero mean stationary fluctuating component. Recently failure of structures due to transient events that are temporally and spatially small, and characterized by non-stationary wind speed fluctuations are being documented. One of these transient events that are documented to be responsible for the failure of light slender structures is downburst outflows. In the past 20 years, Wind excited response of structures due to downburst outflows has been studied using wind speed data, wind tunnel simulations, and computational fluid dynamics applications. These studies resulted in analytical approaches for the wind field model and dynamic excitation calculation. However, unlike synoptic winds, there is no design approach that is collectively agreed upon by researchers and codified in guidelines for design against downburst winds.

Full-scale wind and structural response monitoring is practiced in wind engineering since the earliest construction of tall structures. It has been used to validate theoretical design approaches and wind tunnel testing procedures against atmospheric boundary layer winds. Its application for small-scale events such as downburst outflows is difficult because of the unpredictability of the occurrence of these events. In addition, their small spatial and temporal scale also make the selection of the monitoring site difficult because the probability of registering a downburst event at the monitored structure can not be predicted with high certainty. On the other hand, the validation of the analytical models of downburst wind can not rely on wind tunnel and computational fluid dynamics simulations because of the unavailability of 3-D wind field data during downbursts. This makes full-scale wind and structural response monitoring of structures the most reliable method of validating theoretical models. In light of this, continuous long-term monitoring of the wind-and-structural response of three slender structures was implemented by the GS-WinDyn research team at the University of Genova. The study presented in this

dissertation focuses on one of the three monitored structures which is a slender lighting pole located in La Spezia, Italy. First, the ambient vibration data of the structure was used to investigate the dynamic properties of the structure through operational modal analysis. Then, case studies of downburst events were extracted from the registered monitoring data to analyze the wind and structural response during these events and to investigate the correlation between wind speed and structural response parameters. The response of the structure was calculated in the time domain considering simplified models and assumptions for the wind field and aerodynamic loading. The result was compared with the registered response of the structure to highlight the level of uncertainties in the considered models and assumptions. Furthermore, a detailed review and validation of selected analytical dynamic response calculation methods, that have a complete framework for engineering applications, was done. The simplicity of the monitored structure, and the possibility of obtaining both the quasi-steady and resonant components of the structural response using strain registrations, will make this study a benchmark for the validation of methods and simulations of downburst wind load and response.

Table of contents

List of figures

List of tables

Nomenclature

Acronyms / Abbreviations

ABL Atmospheric boundary layer

CFD Computational fluid dynamics

EPSD Evolutionary power spectral density

EWST Equivalent wind spectrum technique

FDD Frequency domain decomposition

FD Frequency decay

FRF Frequency response function

G-GFF Generalized gust front factor

GRF Gust response factor

MAC Modal assurance criteria

MDOF Multiple degree of freedom

MEMS Micro-electro-mechanical system

OMA Operational modal analysis

POD Proper orthogonal decomposition

PSD Power spectral density

RDS Random decrement signature

RMS Root mean square

SDOF Single degree of freedom

SD Spectral density

TRS Thunderstorm response spectrum

TRST Thunderstorm response spectrum technique

Chapter 1

Introduction

1.1 State of the art

Wind events might vary from large-scale phenomena such as extratropical cyclones to small-scale events such as tornadoes and thunderstorm outflows but regardless of their causal, they are present all over the world. Structures need to be designed considering the expected wind actions at the location. For more than six decades the design of structures against wind actions was focused on the synoptic events that are characterized by large scale, long duration, and approximately straight-line wind. A major breakthrough in the design of structures against the synoptic wind was in 1961 when Alan D. Davenport conceptualized the well-known Davenport chain. Consequently, design guidelines and codes incorporated detailed procedures for the calculation of wind actions. However, the framework is built on the assumption of a wind speed time history that results in a zero mean stationary fluctuation when the mean wind speed averaged over 10 minutes to 1 hour is subtracted. This is true for large-scale synoptic events but small-scale events such as tornadoes and downbursts usually last not more than a few minutes and the wind speed time history is characterized by a transient non-stationary property. Thus, the framework of wind excited response of structures calculation for synoptic winds characterized by stationary fluctuation might not be appropriate for application in transient non-stationary winds. In recent years, many economical losses due to small-scale events resulting from convective activities such as tornadoes and downbursts are being documented. Thus the need to incorporate such small-scale events in the design guidelines and frameworks is being recognized.

One of the small-scale wind events that are responsible for economic loss in many mixed-climate regions is a downburst outflow. It is defined by Fujita as " A downburst is one of the small-scale meteorological events in which a downdraft of air impinges on the earth's surface creating a radial outflow" (Fujita, 1985). The formation of downbursts is described in Chay and

Letchford (2002) as "Fundamentally, convection drives an updraft, which transports warm moist, more buoyant, air to great elevations. Subsequently, the moisture in this air condenses, cools, and the upward motion is halted. The now colder more dense air begins to accelerate toward the ground as a downdraft. Downbursts occur when a strong downdraft collides with the surface of the earth and diverges. Close to the point of impact, the flow resembles that of a wall jet. As the flow spreads out over the ground it behaves as a gravity or density current. The flow field created by such an event, particularly near the impact point, varies from an atmospheric boundary layer wind field in a number of fundamental ways". The flow structure can be better visualized from Hjelmfelt's (Hjelmfelt, 1988) summary of the JAWS result shown in Fig. 1.1

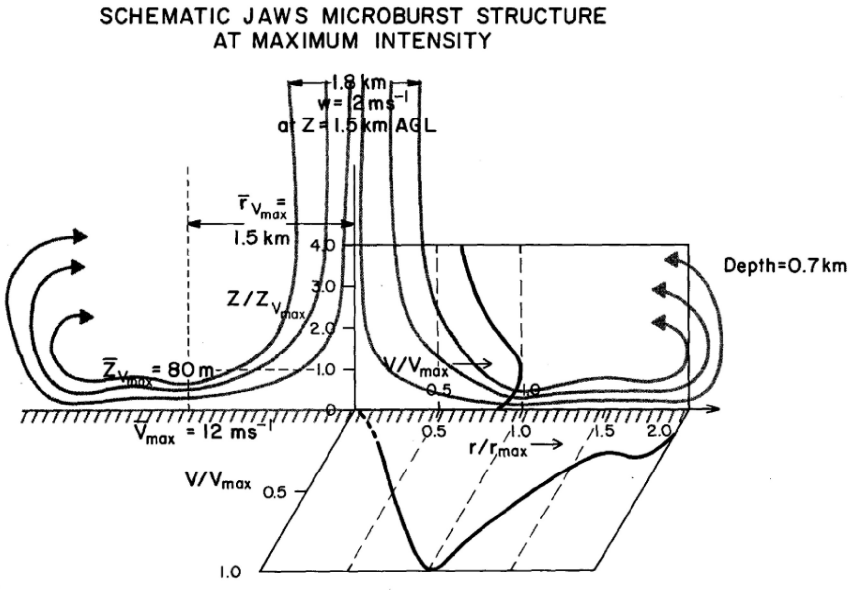

Fig. 1.1 Velocity profile of a typical microburst during JAWS (From Hjelmfelt (1988))

The study of downburst wind effects on structures was not widely addressed in literature due to the scarcity of wind speed data and the complexity of the problem due to the transient property. However, in the past 20 years, many researchers have studied the modeling and simulation of downbursts through analytical models, wind tunnel tests, and computational fluid dynamics (CFD) simulations. In addition, the wind-excited response of structures was also studied through numerical and analytical methods. In the following sub-sections, the state of the art in the modeling of downburst wind and the wind-excited response of structures is presented. It should be underlined that many researchers have exerted tremendous effort to address this topic through wind tunnel and CFD simulations (Aboshosha et al., 2015; Asano et al., 2019; Butler et al., 2008; Elawady et al., 2018; Junayed et al., 2019; Kim and Hangan, 2007; Le and Caracoglia, 2019; Mason et al., 2005; McConville et al., 2009; Romanic et al., 2019; Sengupta et al., 2008;

Vermeire et al., 2011). However, since the scope of this dissertation is limited to analytical techniques, the state of the art is focused on only analytical approaches.

1.1.1 Analytical modeling of downburst wind

Choi and Hidayat (2002a) were the first to indicate that the classical approach of modeling the wind speed as a summation of a constant mean wind speed averaged over 10 minutes to 1 hr and a stationary fluctuating component might underestimate the wind-excited response of structures under downbursts. They calculated the alongwind response of a single degree of freedom (SDOF) structure to a downburst wind record in the time domain and compared the result with the peak response calculated using the classical approach of the gust response factor. They suggested that the mean wind speed should be time-varying and it should be extracted through a running/moving window of fixed length. The research after this indication was all based on a time-varying mean although its definition differs among studies. Thus the mean wind speed was modeled as a time and height-varying parameter. The time-varying mean wind speed was further defined as a product of a time function and a height function (the vertical profile) in Chen and Letchford (2004a) indicating that the shape of the mean wind speed vertical profile is not changing in time.

The time-varying mean wind speed was extracted from real or wind tunnel simulated thunderstorm wind speed records (Brusco et al., 2019; Chen and Letchford, 2004b, 2005, 2006, 2007; Roncallo and Solari, 2020; Solari, 2016; Solari and De Gaetano, 2018; Solari et al., 2015b, 2017). The extraction of the time-varying mean wind speed was through the use of the wavelet shrinkage method in Chen and Letchford (2005, 2006, 2007), and a running average using a constant moving window of fixed length in Choi and Hidayat (2002a); Solari (2016); Solari and De Gaetano (2018); Solari et al. (2015b). The length of the constant window was recommended to be 60 seconds in Choi and Hidayat (2002a), and 17 or 34 seconds in Lombardo et al. (2014). Solari et al. (2015a) studied the length of the constant window using 93 thunderstorm wind speed records and quantifying the harmonic content shared by the mean and fluctuating components, they recommended a window of 30 seconds. Tubino and Solari (2020) studied the effect of adopting different windowing techniques for separating the slowly varying mean and fluctuating components. They interpreted the running averaging method as a kernel regression with a uniform window modulating function. Through this interpretation, they studied the harmonic components and the power spectral densities of the wind components considering constant, Gaussian, and Cardinal sine functions.

In other studies where sufficient records of wind speed during downbursts are not available or simplification of the wind speed model was desired, the time function of the mean wind speed,

which is the ratio of the mean wind speed time history and the maximum mean wind speed, was modeled by a simplified sine, cosine, exponential, and sawtooth-like functions (Kwon and Kareem, 2009, 2013, 2019; Le and Caracoglia, 2015a,b, 2017). The 3D wind speed model by Holmes and Oliver (2000) considering storm translation was also used for the time variation of the mean wind speed in some studies (Chen and Letchford, 2004a; Le and Caracoglia, 2017).

The vertical profile of wind speed during downbursts is usually considered to be "nose shaped" with a wind speed profile that increases with height up to a certain height attaining its maximum value and decreases upwards. This led to the hypothesis that low-rise structures might be subject to higher wind loads than high-rise structures in the case of downburst outflows (Chay and Letchford, 2002). Two models of the vertical profile of downburst wind speed are common in the literature. The first one is Vicroy's model, which was initially derived from the mass continuity equations by Oseguera and Bowles (1988) and modified by Vicroy (1991) and Vicroy (1992). The second model is Wood's model which is an empirical model derived using wind tunnel simulations of downbursts by Wood and Kwok (1998) and Wood et al. (2001). Vicroy's model was applied in Kwon and Kareem (2009, 2013, 2019); Le and Caracoglia (2015b) while Wood's model was applied in Brusco et al. (2019); Chen and Letchford (2004a); Solari et al. (2017). Proper orthogonal decomposition (POD) was used to study the vertical profile of the mean wind speed during two downburst events in Chen and Letchford (2005). By fitting the eigenvectors of the 1^{st} coefficients obtained through the proper orthogonal decomposition (POD) to Wood's model, they found the maximum wind speed and the height to the maximum wind speed (Chen and Letchford, 2007). Although this was done for only two case studies of downbursts, they recommended this approach be used on a large wind speed database for the proposition or modification of the empirical wind speed profile model of downbursts. More recently, the vertical profile of the mean wind speed was studied using downburst wind speed data at various heights obtained through Lidar profilers in Canepa et al. (2020) and it was shown that the vertical profile varies in time and the classical nose shape profile is eminent mainly during the velocity ramp-up and peak stages. The analytical model that simulates the horizontal mean wind speed due to a translating downburst proposed by Xhelaj et al. (2020) is expected to be applied for future structural response studies because it addresses the coupling between background ABL wind and translating downburst.

Chen and Letchford (2004a) modeled the time-varying fluctuating wind speed as a zero mean, non-stationary component which is a product of a modulation function and a normalized Gaussian fluctuation of unit variance. Consequently, researchers followed this approach with different assumptions for the modulation function and for the normalized fluctuation. In most of the literature, the modulation function is assumed to be a function of time, indicating that the fluctuating wind speed is a uniformly modulated stationary process. The modulation function

was considered as 1% to 25% of the time function of the mean wind speed in Chen and Letchford (2004a) and Chay and Albermani (2005) while it was considered to be 15% in Le and Caracoglia (2015b). On the other hand, the modulation function was introduced to be the time-varying standard deviation of the fluctuating wind speed in Chen and Letchford (2005) and it was found using a two-staged filter (Chen and Letchford, 2005, 2007). Solari et al. (2015a) followed a similar approach and defined the modulation function as the standard deviation of the fluctuating wind speed component but it was obtained by calculating the moving standard deviation over a window of 30 seconds. This approach of calculating moving standard deviation was applied in consecutive research (Brusco et al., 2019; Solari, 2016; Solari and De Gaetano, 2018; Solari et al., 2015b, 2017). Recently, the assumption of the fluctuating wind speed as a uniformly modulated stationary process was verified by Roncallo and Solari (2020) by analyzing the time variation of the up-crossing rate of the residual turbulent fluctuation using numerous downburst wind records. The choice of the wind speed time function or the standard deviation time function as a modulating function of the fluctuating wind speed was also studied using statistical analysis of 129 thunderstorm records in Roncallo and Solari (2020). It was concluded that the time function of the mean wind speed is a better alternative for a modulating function of the fluctuating wind speed.

The concept of time-varying turbulence intensity calculated as the ratio between the time-varying standard deviation and the time-varying mean was introduced in Chen and Letchford (2005). However, they have also underlined that the time-varying turbulence intensity will not give the same physical meaning as the case of atmospheric boundary layer (ABL) winds. By studying the time-varying turbulence intensity of two downburst events through the POD, they suggested that the turbulence intensity can be considered as a time-invariant parameter because it fluctuates around its mean value. Consequently, in Chen and Letchford (2007), the turbulence intensity was considered to be time-invariant represented by the mean of its time-varying value. As a result, many researchers assumed the turbulence intensity to be a time-invariant constant (Kareem et al., 2019; Kwon and Kareem, 2009, 2013). Solari et al. (2015a) calculated the time-varying turbulence intensity for 93 downburst records and noted that it is a weakly-dependent function of time. However, they raised questions over the appropriateness of using the mean of the time-varying turbulence intensity because of its asymmetrical distribution. In addition, since the time-varying turbulence intensity modulates the normalized fluctuating component, they have also called for future assessment on the implication of removing the time modulation of the normalized fluctuating component by considering constant turbulence intensity. This uncertainty was further investigated by Roncallo and Solari (2020) in which the effect of the time-invariant turbulence intensity represented by its mean is studied by calculating the dynamic response of SDOF systems with various damping and natural frequencies to 129 thunderstorm

records. It was shown that the consideration of time-invariant turbulence intensity will result in an overestimation of the alongwind response by not more than 10%.

The profile of the turbulence intensity was studied through POD in Chen and Letchford (2005) and in Chen and Letchford (2007), and the profile of the turbulence intensity of ABL winds given ASCE 7-98 (1998) was considered to be applicable for downburst winds. The eigenvectors obtained from POD were fitted to the empirical model given in ASCE 7-98 (1998) to calculate the turbulence intensity at 10 meters. The results showed that the turbulence intensity at 10m in the case of the considered two downbursts was smaller than the expected value under ABL winds. However, it should be noted that this indication was based on an analysis of two downburst records measured by a tower whose maximum measurement height was 15 m. Similarly, Kwon and Kareem (2009) also adopted the empirical formula of the turbulence intensity of ABL winds for downburst winds. Canepa et al. (2020) has studied the vertical profile of the turbulence intensity using wind speed measurements at various heights and could not find a defined behavior because the profile changes in time.

The normalized fluctuation was assumed as stationary and Gaussian in Chay and Albermani (2005); Chen and Letchford (2004a). However, Chen and Letchford (2005) showed that the normalized fluctuation might not be stationary and they called for further investigation. Besides, the power spectral density (PSD) of the normalized fluctuation was assumed to be similar to the PSD of fluctuating wind in ABL winds in many research (Chay and Albermani, 2005; Chen and Letchford, 2004a; Kwon and Kareem, 2009, 2013, 2019; Le and Caracoglia, 2017). With the availability of downburst wind data through a network of anemometers, Solari et al. (2015a) showed that the normalized fluctuation is indeed Gaussian, and in the inertial sub-range, it has a similar PSD as the fluctuating component in ABL winds.

Chen (2008) was the first to define the fluctuating wind speed component of transient events in the time-frequency domain. The fluctuating wind component was defined as a zero mean evolutionary random process which is modeled as a zero mean stationary process modulated with a complex-valued deterministic modulation function. The modulating function is defined as a function of time, frequency, and height.

Due to the absence of measured data, the coherence function of the normalized fluctuating component was mostly considered to be similar to the coherence function of ABL winds given by Davenport (Brusco et al., 2019; Chen and Letchford, 2007; Kwon and Kareem, 2009, 2013, 2019; Le and Caracoglia, 2015b; Solari, 2016; Solari and De Gaetano, 2018; Solari et al., 2017). Chen and Letchford (2005) tried to estimate the exponential decay coefficients of the Davenport coherence function by analyzing the wind speed records at various heights during two downburst events through the application of POD. Most recently, Peng et al. (2018) defined the coherence function as a time-varying function obtained using the cross-evolutionary

power spectral density (EPSD) of normalized fluctuations at various heights. They proposed a modification to Davenport's coherence function for application in downburst winds. They indicated that the coherence function should be a function of the time-varying standard deviation of fluctuation instead of the time-varying wind speed. In addition, they obtained time-varying exponential functions by fitting the modified coherence function to the obtained coherence values. However, they have underlined that this definition of the time-varying coherence function is not feasible for engineering applications and an equivalent coherence function should be investigated.

In the studies where the mean wind speed is extracted from the recorded wind speed time history, the crosswind component of wind speed and the directional change that is evident in downburst wind records were not considered. As a result, studies on the response of structures to downburst events did not consider the crosswind response and the time variation of wind direction. Highlighting the importance of these neglected aspects, Zhang et al. (2019) introduced the directional decomposition approach. In this approach, the wind speed is decomposed into time-varying mean component in the alongwind direction, and fluctuating component in the alongwind as well as crosswind direction.

1.1.2 Aerodynamic load due to downburst winds

In atmospheric boundary layer winds, the quasi-steady theory is widely used to map the wind speed to wind pressure on the surface of the structure. The quasi-steady theory assumes that the pressure fluctuation on the structure is directly proportional to the wind velocity fluctuation upstream. In this approach, the cross-correlation of velocity and pressure is unity and the peak pressure or load occurs at the instant of the maximum wind velocity (Letchford et al., 1993). In all the studies reviewed in this dissertation that addressed downburst wind loading and response, quasi-steady theory has been applied.

The need for a critical assessment of abrupt changes in the wind field magnitudes and associated modifications in the aerodynamics of structures during transient events has been emphasized as a current challenge by Kareem and Wu (2013). The validity of the quasi-steady theory for application in transient winds such as downbursts and tornadoes has been questioned in the research by Hangan et al. (2019). The main underlying assumptions of the quasi-steady theory were presented as (1) fluctuations in the surface pressures are only due to the wind inflow velocity fluctuations; (2) the upstream wind velocity is steady and can be decomposed using Reynolds decomposition; and (3) the velocity fluctuations are much smaller compared to the mean flow. These assumptions were discussed considering the influence of the presence of the structure on the flow turbulence in small-scale events, the difficulty of decomposing the wind

speed using the classical Reynold's decomposition, and the applicability of the small turbulence assumption in events such as tornadoes and downbursts.

Early research by Sarpkaya (1963), Sarpkaya (1966), and Sarpkaya and Ihrig (1986) on cylinders and rectangular prisms in unsteady flows indicated an overshoot in the aerodynamic force during unsteady flows. Takeuchi and Maeda (2013) studied the aerodynamics of elliptic cylinders subjected to accelerating and steady flow and showed that the overshooting in the aerodynamic force is dependent on the rise time/ acceleration of the flow. Consequently, Yang and Mason (2019) studied the aerodynamics of rectangular cylinders under steady and accelerating wind flow with the acceleration rate scaled to that experienced during strong downbursts and showed that the drag and lift coefficients during accelerating wind flow are generally small in accelerating flow conditions. Brusco et al. (2022) extracted time-varying acceleration from the wind speed measurements using continuous wavelet and studied the effect of added mass due to the acceleration of the flow applying quasi-steady theory and concluded that the effect is very small unless the structure is elongated in the direction of the flow or the wind speed is very low. However, the possible consequence of a different shedding of vortices in the wake during unsteady flows on the aerodynamic load was also emphasized (Brusco, 2021).

Thus, it should be noted that a generally accepted theory for mapping wind speed to wind pressure in transient winds, particularly downbursts winds, is not available and the existing research on the response of structures during downburst winds is based on the application of quasi-steady theory.

1.1.3 Wind-excited response of structures due to downburst winds

The wind-excited response of structures has been studied by researchers in the time domain, frequency domain, and time-frequency domain with the aim of proposing analysis approaches and studying the effect of different wind loading parameters.

The wind-excited response of SDOF systems was calculated in the time domain in Choi and Hidayat (2002b) to highlight the underestimation of response when the classical approach of the gust response factor is applied to the downburst excited response of SDOF systems. The response of a cantilever multiple degrees of freedom (MDOF) structure to a simulated downburst wind speed time history was calculated in the time domain by Chen and Letchford (2004a) to study the effect of the level of correlation of the wind field in the vertical direction. Chen and Letchford (2004b) defined a parameter called "maximum dynamic magnification factor" which is the ratio between the maximum dynamic response and the maximum static response. This parameter was calculated for the downburst excited response of the CAARC building in the time domain, considering different assumptions of time and height function for the wind speed,

and varying the structural damping and natural frequency. Similarly, the response of a single degree of freedom system to simulated downburst winds was calculated in the time domain by Chay and Albermani (2005) to compare the dynamic response factor of SDOF systems subjected to downburst winds and ABL winds. They found out that the dynamic response factor (DRF) during downbursts is equal to or lower than the DRF in ABL winds.

Holmes et al. (2005) proposed the idea of a response factor whose interpretation is analogous to the response spectrum technique in earthquake engineering. The response factor was calculated for SDOF systems by solving the equation of motion in the time domain. This idea was strengthened and applied by Solari et al. (2015b) in which 93 thunderstorm wind speed records collected through a closely spaced network of anemometers were used to generate the thunderstorm response spectrum curves for SDOF systems. This was further extended to multiple degree of freedom (MDOF) systems in Solari (2016) and Solari and De Gaetano (2018).

Chen (2008) defined the fluctuating response under transient winds in the time-frequency domain. He created a framework for calculating the alongwind response and defined the EPSD and time-varying root mean square (RMS) of the fluctuating response. The framework was applied to study the response of a tall building under a downburst and synoptic winds (Chen, 2008).

Kwon and Kareem (2009) introduced a new framework for wind load effects on structures. The framework puts the wind load calculation of synoptic and transient events under a single umbrella. They defined the gust front factor that accounts for the variation in the vertical profile of wind speed, dynamic effects due to a sudden increase in wind speed, nonstationarity of the turbulence, and transient aerodynamics. The gust front factor simply reduces to the classical gust loading factor in the case of synoptic winds. In Kwon and Kareem (2013), the generalized gust front factor which accounts for the dynamic effect in downburst winds is introduced for easier integration with international standards. In addition, a closed-form solution obtained through frequency domain analysis and EPSD was also given for the root mean square (RMS) of fluctuating response considering long-duration storm. Furthermore, in Kwon and Kareem (2019) a closed-form solution is given for the mean peak factor, and a comparison of the gust front factor approach with the thunderstorm response spectrum method is made. Similarly, Roncallo et al. (2022) studied the maximum dynamic response of SDOF systems based on the evolutionary spectral model. The RMS of the fluctuating response and the peak factor were defined with and without the simplification resulting from the assumption of long duration storm. In addition, a correction factor was introduced to address the overestimation of the maximum response in lowly damped systems due to the peak factor defined by Davenport.

On the other hand, the study on the dynamic response of structures against transient wind loads considering motion-induced loads (aeroelasticity) was studied in Le and Caracoglia (2015b).

They applied the Wavelet-Galerkin method to solve the equation of motion of a tall building subjected to transient and synoptic wind considering the motion-dependent loads. This study was further extended to consider nonlinearity in damping and stiffness in Le and Caracoglia (2015a). Furthermore, the dynamic response of the CAARC building due to a digitally simulated Andrews AFB thunderstorm was studied using the Wavelet-Galerkin approach in Le and Caracoglia (2017).

In Brusco and Solari (2021), the time-domain formulation of the dynamic response of slender structures to synoptic events considering motion-induced force is generalized to thunderstorm outflows. The generalization considered the change in wind direction that is evident in thunderstorm outflows. The crosswind response of a slender structure to thunderstorm outflows was calculated using the generalized framework and it was shown that the irregular trend of the wind direction prevents the building up of large oscillations due to motion-induced force.

Peng et al. (2018) calculated the alongwind response of a tall building in the frequency domain considering a time-varying coherence function obtained from the evolutionary power spectral density of the fluctuating wind at various heights. However, it was concluded that an equivalent time-invariant coherence function derived from the time-varying coherence function is more feasible for engineering applications.

In most studies concerning the response of structures to downburst winds, the wind speed was modeled as having a time-varying mean and fluctuating components in the alongwind direction. This approach, which is referred to as the classical decomposition approach, did not consider the crosswind component of wind speed, and the change in wind direction. After the introduction of the directional decomposition approach by Zhang et al. (2019), the implication of adopting the classical decomposition technique in the dynamic response of slender structures was studied by Brusco et al. (2019). The response of two slender structures to 10 records of downburst wind speeds was studied in the time domain considering the classical and directional decomposition techniques. The response of the non-polar symmetric structure showed an increase of up to 17% when the directional decomposition technique is applied instead of classical decomposition.

1.1.4 Full-scale monitoring of structures

Full-scale monitoring of structures during downburst outflows is not widely available in literature because of the small spatial and temporal scale of downbursts. Stengel and Thiele (2017) presented the first study conducted through full-scale monitoring of a structural response during a downburst. They studied the sway angle of an overhead transmission line during a downburst using full-scale wind and structural response monitoring. They have shown that the time-varying mean sway angle of the transmission line estimated using time domain analysis and registered

by the monitoring system are in close agreement with each other. Lombardo et al. (2018) studied the aerodynamics of a low-rise building during the downburst event of June 2003 using full-scale pressure measurement on the walls and roof of a monitored building at Texas Tech University. They compared the loading characteristics during the downburst event with data from the same building for the previous 128 ABL wind events. It was indicated that, in general, the observed pressure coefficients are below the threshold measured during ABL winds. Recently, Zhang et al. (2022) presented a study on an ultra-long stay cable during a transient event using full-scale data registered by the structural health monitoring system.

1.2 Statement of the problem

In the previous section, it was highlighted that many researchers explored various approaches for downburst modeling and the wind-excited response of structures. However, it should also be noted that the analytical wind modeling and wind-excited response calculation approaches have not been validated with full-scale monitoring of structures under downbursts. Literature is rare on the full-scale monitoring of structures under transient events. Particularly, monitoring data on the dynamic response of real, slender structures under downburst winds is not available. Because of the complexity of downburst events and the difficulty of simulating their wind field in a conventional boundary layer wind tunnels, full-scale simultaneous monitoring of wind and structural response is the most reliable approach to validate analytical models and methods. In light of this, the GS-WinDyn research group at the University of Genova has initiated long-term full-scale monitoring of selected three slender structures through the European Union-funded project, THUNDERR (Solari, 2020). The full-scale monitoring aims to study the response of slender structures under downburst winds and build benchmark cases for validation of numerical and analytical methods of downburst wind loading. To achieve this goal, simple slender structures with minimal uncertain structural properties, located in geographical sites known for a previous recurrent history of downburst events, are monitored. The continuous, long-term monitoring campaign enabled the simultaneous measurement of wind and structural response during thunderstorm outflows with a high frequency of sampling rate.

1.3 Objective and scope of the research

The aim of the research is to study the dynamic response of structures under downburst winds using full-scale simultaneous measurement of wind and structural response of a slender structure.

It is also intended to validate selected analytical downburst wind load calculation techniques using the registered data during downburst events.

The scope of the study covers

- analysis of selected wind speed and structural response parameters to study the correlation between wind speed and structural response parameters during case studies of downbursts
- calculation of the response of the structure in the time domain using the wind speed measurement of cases studies of downbursts and comparison of the result with the registered response of the structure to study the effect of the considered assumptions in the aerodynamic loading and response calculation
- review, comprehensive comparison, and validation using registered data of selected two analytical downburst wind load calculation methods that have a complete framework for engineering application and codification

1.4 Organization of the dissertation

The dissertation is organized into five chapters.

In Chapter 2, the system identification of the monitored structure is addressed. First, the geometry of the monitored structure and its sensors are introduced. Then the dynamic properties of the structure are investigated using ambient vibration data registered by the monitoring system. The aerodynamic property of the structure studied by Orlando et al. (2023) is also reported for the sake of completeness.

In Chapter 3, The registered wind data is analyzed to identify the occurrence of downburst events. From the identified downburst events, those with significant intensity are selected as case studies for further assessment. The structural response registered during the selected case studies of downbursts is analyzed and reflections regarding the correlation between the response of the structure and important wind parameters are made.

In Chapter 4, the response of the structure is numerically calculated in the time domain using the wind speed measurement during the selected downburst case studies considering different assumptions for the wind field and aerodynamic loading. The calculated response time history is then compared with the registered response time history to highlight the implications of the considered assumptions.

In Chapter 5, two main analytical downburst wind load calculation techniques that have a complete framework feasible for engineering application and codification are selected for

validation. First, the two approaches are studied and a comprehensive comparison between them is made from a theoretical point of view. Then, the two methods are validated by calculating the response of the monitored structure to the wind speed measured during the selected case studies of downbursts and comparing the result with the registered response.

References

Aboshosha, H., Bitsuamlak, G., and El Damatty, A. (2015). Turbulence characterization of downbursts using LES. *J. Wind Eng. Ind. Aerodyn.*, 136:44–61.

Asano, K., Iida, Y., and Uematsu, Y. (2019). Laboratory study of wind loads on a low-rise building in a downburst using a moving pulsed jet simulator and their comparison with other types of simulators. *J. Wind Eng. Ind. Aerodyn.*, 184(June 2018):313–320.

ASCE 7-98 (1998). Minimum design loads for buildings and other structures.

Brusco, S. (2021). *Transient phenomena induced by thunderstorm out?ows on slender structures*. PhD thesis, University of Genova.

Brusco, S., Buresti, G., and Piccardo, G. (2022). Thunderstorm-induced mean wind velocities and accelerations through the continuous wavelet transform. *J. Wind Eng. Ind. Aerodyn.*, 221:104886.

Brusco, S., Lerzo, V., and Solari, G. (2019). Directional response of structures to thunderstorm outflows. *Meccanica*, 54(9):1281–1306.

Brusco, S. and Solari, G. (2021). Transient aeroelasticity of structures subjected to thunderstorm outflows. *Eng. Struct.*, 245.

Butler, K., Cao, S., Tamura, Y., Ozono, S., and Kareem, A. (2008). Characteristics of surface pressures on prisms immersed in a transient gust front flow field. In *BBAA VI Int. Colloq. Bluff Bodies Aerodyn. Appl. Milano, Italy, July 20-24*.

Canepa, F., Burlando, M., and Solari, G. (2020). Vertical profile characteristics of thunderstorm outflows. *J. Wind Eng. Ind. Aerodyn.*, 206(August).

Chay, M. and Albermani, F. (2005). Dynamic Response of a SDOF System Subjected to Simulated Downburst Wind. *Proc. 6th Asia-Pacific Conf. Wind Eng.*

Chay, M. T. and Letchford, C. W. (2002). Pressure distributions on a cube in a simulated thunderstorm downburst—Part A: stationary downburst observations. *J. Wind Eng. Ind. Aerodyn.*, 90(7):711–732.

Chen, L. and Letchford, C. W. (2004a). A deterministic-stochastic hybrid model of downbursts and its impact on a cantilevered structure. *Eng. Struct.*, 26(5):619–629.

Chen, L. and Letchford, C. W. (2004b). Parametric study on the along-wind response of the CAARC building to downbursts in the time domain. *J. Wind Eng. Ind. Aerodyn.*, 92(9):703–724.

Chen, L. and Letchford, C. W. (2005). Proper orthogonal decomposition of two vertical profiles of full-scale nonstationary downburst wind speeds. *J. Wind Eng. Ind. Aerodyn.*, 93(3):187–216.

Chen, L. and Letchford, C. W. (2006). Multi-scale correlation analyses of two lateral profiles of full-scale downburst wind speeds. *J. Wind Eng. Ind. Aerodyn.*, 94(9):675–696.

Chen, L. and Letchford, C. W. (2007). Numerical simulation of extreme winds from thunderstorm downbursts. *J. Wind Eng. Ind. Aerodyn.*, 95(9-11):977–990.

Chen, X. (2008). Analysis of Alongwind Tall Building Response to Transient Nonstationary Winds. *J. Struct. Eng.*, 134(5):782–791.

Choi, E. C. and Hidayat, F. A. (2002a). Dynamic response of structures to thunderstorm winds. *Prog. Struct. Eng. Mater.*, 4(4):341–430.

Choi, E. C. and Hidayat, F. A. (2002b). Gust factors for thunderstorm and non-thunderstorm winds. *J. Wind Eng. Ind. Aerodyn.*, 90:1683–1696.

Elawady, A., Aboshosha, H., and Damatty, A. E. (2018). Aero-elastic response of transmission line system subjected to downburst wind: Validation of numerical model using experimental data Seismic Analysis of high rise buildings View project. *Wind Struct.*, 27(2):71–88.

Fujita, T. (1985). The downburst-Micoburst and Macroburst Report of Projects NIMROD and JAWS. *Rep. Proj. NIMROD JAWS*, page 128.

Hangan, H., Romanic, D., and Jubayer, C. (2019). Three-dimensional, non-stationary and non-Gaussian (3D-NS-NG) wind fields and their implications to wind–structure interaction problems. *J. Fluids Struct.*, 91:102583.

Hjelmfelt, M. R. (1988). Structure and life cycle of microburst outflows observed in colorado. 27:090–927.

Holmes, J., Forristall, G., and Mcconochie, J. (2005). Dynamic response of structures to thunderstorm winds. *10th Am. Conf. Wind Eng. ACWE 2005*, (July 2017).

Holmes, J. D. and Oliver, S. E. (2000). An empirical model of a downburst. *Eng. Struct.*, 22(9):1167–1172.

Junayed, C., Jubayer, C., Parvu, D., Romanic, D., and Hangan, H. (2019). Flow field dynamics of large-scale experimentally produced downburst flows. *J. Wind Eng. Ind. Aerodyn.*, 188(March):61–79.

Kareem, A., Hu, L., Guo, Y., and Kwon, D. K. (2019). Generalized wind loading chain: Time-frequency modeling framework for nonstationary wind effects on structures. *J. Struct. Eng.*, 145(10):04019092.

Kareem, A. and Wu, T. (2013). Wind-induced effects on bluff bodies in turbulent flows: Nonstationary, non-Gaussian and nonlinear features. *J. Wind Eng. Ind. Aerodyn.*, 122:21–37.

Kim, J. and Hangan, H. (2007). Numerical simulations of impinging jets with application to downbursts. *J. Wind Eng. Ind. Aerodyn.*, 95(4):279–298.

Kwon, D. K. and Kareem, A. (2009). Gust-front factor: New framework for wind load effects on structures. *J. Struct. Eng.*, 135(6):717–732.

Kwon, D. K. and Kareem, A. (2013). Generalized gust-front factor: A computational framework for wind load effects. *Eng. Struct.*, 48:635–644.

Kwon, D. K. and Kareem, A. (2019). Towards codification of thunderstorm/downburst using gust front factor: Model-based and data-driven perspectives. *Eng. Struct.*, 199.

Le, T. H. and Caracoglia, L. (2015a). Reduced-order wavelet-Galerkin solution for the coupled, nonlinear stochastic response of slender buildings in transient winds. *J. Sound Vib.*, 344:179–208.

Le, T. H. and Caracoglia, L. (2015b). Wavelet-Galerkin analysis to study the coupled dynamic response of a tall building against transient wind loads. *Eng. Struct.*, 100:763–778.

Le, T. H. and Caracoglia, L. (2017). Computer-based model for the transient dynamics of a tall building during digitally simulated Andrews AFB thunderstorm. *Comput. Struct.*, 193:44–72.

Le, V. and Caracoglia, L. (2019). Generation and characterization of a non-stationary flow field in a small-scale wind tunnel using a multi-blade flow device. *J. Wind Eng. Ind. Aerodyn.*, 186(August 2018):1–16.

Letchford, C. W., Iverson, R. E., and McDonald, J. R. (1993). The application of the Quasi-steady Theory to full scale measurements on the Texas Tech building. *J. Wind Eng. Ind. Aerodyn.*, 48(1):111–132.

Lombardo, F. T., Mason, M. S., and de Alba, A. Z. (2018). Investigation of a downburst loading event on a full-scale low-rise building. *J. Wind Eng. Ind. Aerodyn.*, 182:272–285.

Lombardo, F. T., Smith, D. A., Schroeder, J. L., and Mehta, K. C. (2014). Thunderstorm characteristics of importance to wind engineering. *J. Wind Eng. Ind. Aerodyn.*, 125:121–132.

Mason, M. S., Letchford, C. W., and James, D. L. (2005). Pulsed wall jet simulation of a stationary thunderstorm downburst, Part A: Physical structure and flow field characterization. *J. Wind Eng. Ind. Aerodyn.*, 93(7):557–580.

McConville, A., Sterling, M., and Baker, C. (2009). The physical simulation of thunderstorm downbursts using an impinging jet. *Wind Struct.*, 12(2):133–149.

Orlando, A., Pagnini, L., and Pia Repetto, M. (2023). Wind tunnel tests of a hexadecagonal cylinder with imperfections and ancillaries: aerodynamic characterization and technical discussion. *Eng. Struct.*, 274(March 2022):115114.

Oseguera, R. M. and Bowles, R. L. (1988). A simple, analytic 3-dimensional downburst model based on boundary layer stagnation flow. Technical Report July.

Peng, L., Huang, G., Chen, X., and Yang, Q. (2018). Evolutionary Spectra-Based Time-Varying Coherence Function and Application in Structural Response Analysis to Downburst Winds. *J. Struct. Eng.*, 144(7):1–16.

Romanic, D., LoTufo, J., and Hangan, H. (2019). Transient behavior in impinging jets in crossflow with application to downburst flows. *J. Wind Eng. Ind. Aerodyn.*, 184(November 2018):209–227.

Roncallo, L. and Solari, G. (2020). An evolutionary power spectral density model of thunderstorm outflows consistent with real-scale time-history records. *J. Wind Eng. Ind. Aerodyn.*, 203(April):104204.

Roncallo, L., Solari, G., Muscolino, G., and Tubino, F. (2022). Maximum dynamic response of linear elastic SDOF systems based on an evolutionary spectral model for thunderstorm outflows. *J. Wind Eng. Ind. Aerodyn.*, 224:104978.

Sarpkaya, T. (1963). Lift, drag, and added-mass coefficients for a circular cylinder immersed in a time-dependent flow. *J. Appl. Mech. Trans. ASME*, 30(1):13–15.

Sarpkaya, T. (1966). Separated flow about lifting bodies and impulsive flow about cylinders. *AIAA J.*, 4(3):414–420.

Sarpkaya, T. and Ihrig, C. J. (1986). Impulsively started steady flow about rectangular prisms: Experiments and discrete vortex analysis. *J. Fluids Eng. Trans. ASME*, 108(1):47–54.

Sengupta, A., Haan, F. L., Sarkar, P. P., and Balaramudu, V. (2008). Transient loads on buildings in microburst and tornado winds. *J. Wind Eng. Ind. Aerodyn.*, 96(10-11):2173–2187.

Solari, G. (2016). Thunderstorm response spectrum technique: Theory and applications. *Eng. Struct.*, 108:28–46.

Solari, G. (2020). Thunderstorm Downbursts and Wind Loading of Structures: Progress and Prospect.

Solari, G., Burlando, M., De Gaetano, P., and Repetto, M. P. (2015a). Characteristics of thunderstorms relevant to the wind loading of structures. *Wind Struct. An Int. J.*, 20(6):763–791.

Solari, G. and De Gaetano, P. (2018). Dynamic response of structures to thunderstorm outflows: Response spectrum technique vs time-domain analysis. *Eng. Struct.*, 176(March):188–207.

Solari, G., De Gaetano, P., and Repetto, M. P. (2015b). Thunderstorm response spectrum: Fundamentals and case study. *J. Wind Eng. Ind. Aerodyn.*, 143:62–77.

Solari, G., Rainisio, D., and De Gaetano, P. (2017). Hybrid simulation of thunderstorm outflows and wind-excited response of structures. *Meccanica*, 52:3197–3220.

Stengel, D. and Thiele, K. (2017). Measurements of downburst wind loading acting on an overhead transmission line in Northern Germany. *Procedia Eng.*, 199:3152–3157.

Takeuchi, T. and Maeda, J. (2013). Unsteady wind force on an elliptic cylinder subjected to a short-rise-time gust from steady flow. *J. Wind Eng. Ind. Aerodyn.*, 122:138–145.

Tubino, F. and Solari, G. (2020). Time varying mean extraction for stationary and nonstationary winds. *J. Wind Eng. Ind. Aerodyn.*, 203(October 2019):104187.

Vermeire, B. C., Orf, L. G., and Savory, E. (2011). Improved modelling of downburst outflows for wind engineering applications using a cooling source approach. *J. Wind Eng. Ind. Aerodyn.*, 99(8):801–814.

Vicroy, D. D. (1991). A simple, analytical, axisymmetric microburst model for downdraft estimation. *NASA Tech. Memo. No.104053*.

Vicroy, D. D. (1992). Assessment of microburst models for downdraft estimation. *J. Aircr.*, 29(6):1043–1048.

Wood, G. S. and Kwok, K. C. S. (1998). An empirically derived estimate for the mean velocity profile of a thunderstorm downburst.

Wood, G. S., Kwok, K. C. S., Motteram, N. A., and Fletcher, D. F. (2001). Physical and numerical modelling of thunderstorm downbursts. *J. Wind Eng. Ind. Aerodyn.*, 89(2001):535–552.

Xhelaj, A., Burlando, M., and Solari, G. (2020). A general-purpose analytical model for reconstructing the thunderstorm outflows of travelling downbursts immersed in ABL flows. *J. Wind Eng. Ind. Aerodyn.*, 207:104373.

Yang, T. and Mason, M. S. (2019). Aerodynamic characteristics of rectangular cylinders in steady and accelerating wind flow. *J. Fluids Struct.*, 90:246–262.

Zhang, H., Wang, H., Xu, Z., Zhang, Y., Tao, T., and Mao, J. (2022). Monitoring-based analysis of wind-induced vibrations of ultra-long stay cables during an exceptional wind event. *J. Wind Eng. Ind. Aerodyn.*, 221(July 2021):104883.

Zhang, S., Solari, G., Burlando, M., and Yang, Q. (2019). Directional decomposition and properties of thunderstorm outflows. *J. Wind Eng. Ind. Aerodyn.*, 189(November 2018):71–90.

Chapter 2

System identification

2.1 Introduction

Full-scale monitoring of structural vibration under ambient conditions dates back to the 1930s when investigation on the natural period of structures is made using wind excitation (Hudson et al., 1964; Ward and Crawford, 1966). After the introduction of design guidelines for wind action and the reliance on static and aeroelastic wind tunnel testing, researchers tried to validate wind tunnel testing and the design procedures using full-scale monitoring. The full-scale monitoring of a 57-story building in Canada in which the simultaneous measurement of displacement, strain, acceleration, and surface pressure was made for seven years is one of the earliest examples in which researchers tried to validate the wind load estimation approaches through full-scale monitoring (Dagliesh and Rainer, 1978; Dalgliesh, 1982). Similarly, Jeary et al. (1983) studied the wind-excited response of twelve tall buildings in the UK using full-scale monitoring data. Ohkuma et al. (1991) studied the response of a 68 m building in Japan using full-scale measurement of pressure and acceleration. Littler and Ellis (1992) used the full-scale wind and structural response data collected on a 23-story building in the UK to validate the existing wind response estimation guidelines. Besides buildings, the wind-induced vibration of a transmission line system in Japan was also studied using full-scale monitoring by Momomura et al. (1997).

With the increase in the construction of high-rise and super-tall structures, the full-scale monitoring of these structures through long-term structural health monitoring systems and short-term monitoring during storms has increased (Li et al., 1998, 2004). The full-scale monitoring of three tall buildings in Chicago is one of the notable researches where the wind excited response is studied through long-term monitoring that lasted a decade (Bashor et al., 2012; Kijewski-Correa et al., 2006; Kijewski-Correa and Kochly, 2007; Kijewski-Correa and Pirnia, 2007). Besides the monitoring of structures under extratropical cyclones, literature is also rich in the monitoring of

tall and supertall structures during tropical cyclones (Fu et al., 2012; Li et al., 2006; Li and Wu, 2007; Li et al., 2005, 2003; Wan et al., 2022; Wang and Ni, 2022; Yang et al., 2021). However, the full-scale monitoring of wind excited response of a slender structure during a downburst outflow is not available in the literature. This makes the research presented in this dissertation the first full-scale monitoring study on the downburst wind excited response of a slender structure. The geometric simplicity of the monitored structure makes it very convenient for the validation of analytical wind-excited response calculation methods.

In full-scale monitoring studies, it is common to evaluate the dynamic properties of the structures using ambient vibration data. This is the first step to interpreting the structural response data registered during wind excitation and validating the analytical wind response calculation methods. Thus, in this chapter, the monitored structure is introduced and the dynamic properties of the monitored structure such as the modal frequency, modal shape, and damping ratio are investigated using operational modal analysis techniques.

The geometry and sensors of the monitored slender structure are introduced in Section 2.2. In Section 2.3, the Dynamic properties of the structures are investigated after a brief introduction of the operational modal analysis (OMA) techniques used in this study. Finally, the aerodynamic properties of the structure investigated by Orlando et al. (2023) are reported in Section 2.4.

2.2 Full-scale monitoring of a slender lighting pole

2.2.1 Geometry

The structure selected for wind and structural response monitoring is a 16.6 m-high lighting pole located at the harbor of La Spezia, Italy (Fig. 2.1). The pole is founded on a 2.5 m concrete cube foundation resulting in an almost perfect fixed-end connection allowing no rotation and translation at the base. The structure is made of two hollow steel shafts positioned end to end. At the junction, there is a 1 m overlap where the upper shaft fits over the lower shaft, ensuring a secure connection. Both steel shafts are made through the lamination and calendaring process of a 4 mm thick steel sheet, longitudinally welding the edges of the steel sheets to create a 16-sided hollow polygon section. The bottom shaft starts from the base and extends 7.75 m. It decreases its maximum dimension from 528 mm at the base to 400 mm at the top. The upper shaft starts from 6.75 m from the base of the pole and extends to 16.6 m. It decreases its largest dimension from 417 mm at the bottom to 254 mm at the top. A steel ladder is attached to the pole along the height of the structure on one of the sides of the polygonal shaft and it is interrupted by a rectangular platform at 10 m. At the top of the pole, a square platform houses the anemometer,

lighting equipment, and a security camera. In addition to its self-weight, the pole supports, the attached ladder of mass ≈ 180 kg/m, the intermediate platform of mass ≈ 60 kg, and the top platform with the lighting accessories of mass ≈ 500 kg.

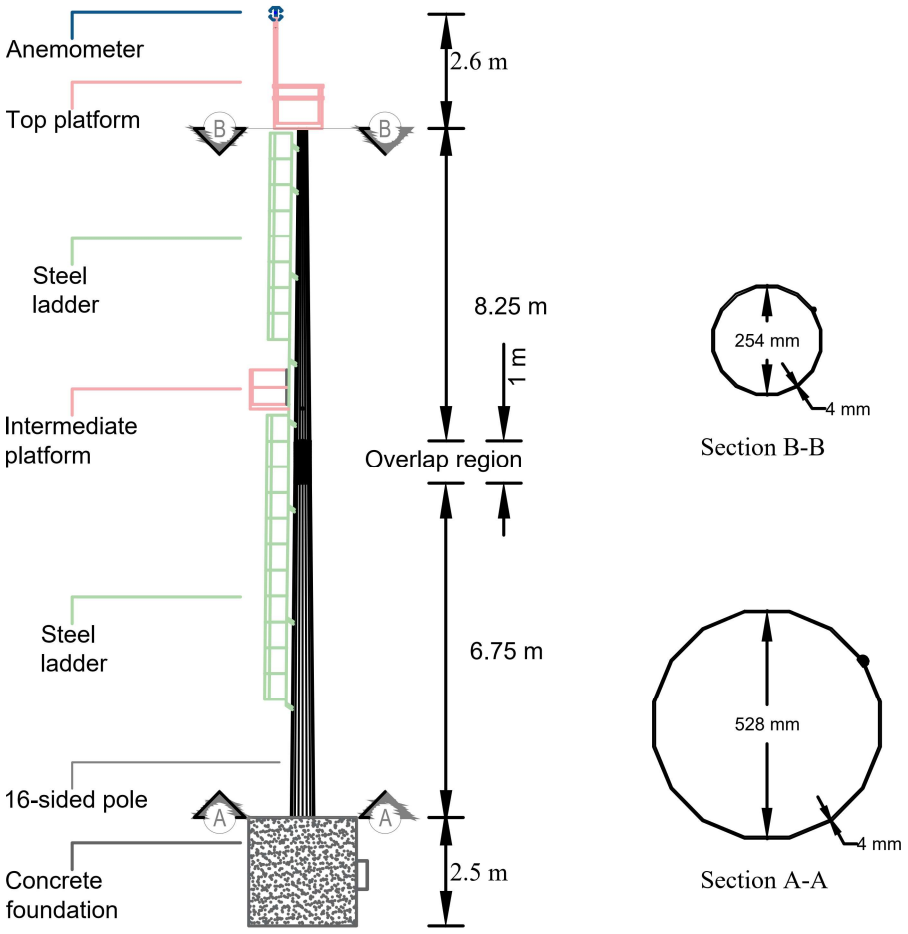

Fig. 2.1 The geometry of the lighting pole

2.2.2 Sensors

The pole is equipped with a monitoring system for long-term, continuous, and simultaneous measurement of wind and structural response. A triaxial ultrasonic anemometer measuring wind speed at a sampling frequency of 10 Hz is installed at 21.7 meters above the ground. The structural response is recorded by accelerometers and strain gauges. Two biaxial micro-electro-mechanical system (MEMS) accelerometers with an operating range of $\pm$ 2 g, measuring acceleration at a sampling frequency of 200 Hz, are installed on one of the sides of the polygonal shafts at 10.5 m and 16.6 m from the base of the pole. Referring to Fig. 2.2, accelerometers A_{x1}

and A_{x2} measure acceleration in the XX direction while accelerometers A_{y1} and A_{y2} measure acceleration in the YY direction. Thus acceleration is measured in the orthogonal axes XX-YY. Eight mono-axial half-bridge strain gauges measuring strain at a sampling frequency of 100 Hz are installed at 0.5m and 1.5 m above the base of the pole on 4 sides of the polygonal shaft. Strain gauges, ε_A, ε_C, ε_E, and ε_G measure strain on the longitudinal axis perpendicular to axis XX while Strain gauges, ε_B, ε_D, ε_F, and ε_H measure strain on the longitudinal axis perpendicular to axis YY. Thus, both the strain gauges and accelerometers are placed on the sides of the polygonal shaft in such a way that response is measured in the two orthogonal directions, XX-YY. The monitoring system has continuously registered wind and structural response data since February 2019 except for periods of interruption due to technical problems.

2.2.3 Remarks on the monitoring system

Best practices in structural response monitoring are available in the literature. Brincker and Ventura (2015) complied detailed guidelines for structural monitoring starting from the inception to the analysis of the registered data. In this section, the monitoring system is evaluated considering the best practices in structural response monitoring, and additional insights specific to the long-term simultaneous measurement of wind and structural response data are given.

- Location of the monitored structure: Because of the small spatial scale of downbursts, initially it was not certain that a downburst outflow will pass through the monitored tower. However, the location of the monitored tower is known for a previous recurring history of downburst events and it was expected that at least a few downburst events will be registered by the monitoring station throughout the long-term monitoring period. On the other hand, the monitored tower location was also ideal because it is mostly free from blockage and obstruction from the wind. The location was also accessible through the port authorities for periodic maintenance and checks. There was a nearby reliable source of electricity and an internet connection for the monitoring system and data transfer.

- Selection of the monitored structure: The monitored tower is simple in terms of geometrical and dynamic properties. This makes it ideal for the validation of analytical methods using registered monitoring data because the wind response can be calculated through analytical methods without major difficulty or without introducing many uncertainties. In addition, the selection of a tower made of a 16-sided polygonal section is optimal because this cross-section is widely available in wind-sensitive structures such as lighting poles, wind turbine towers, antenna masts, power transmission lines, and bridge supports.

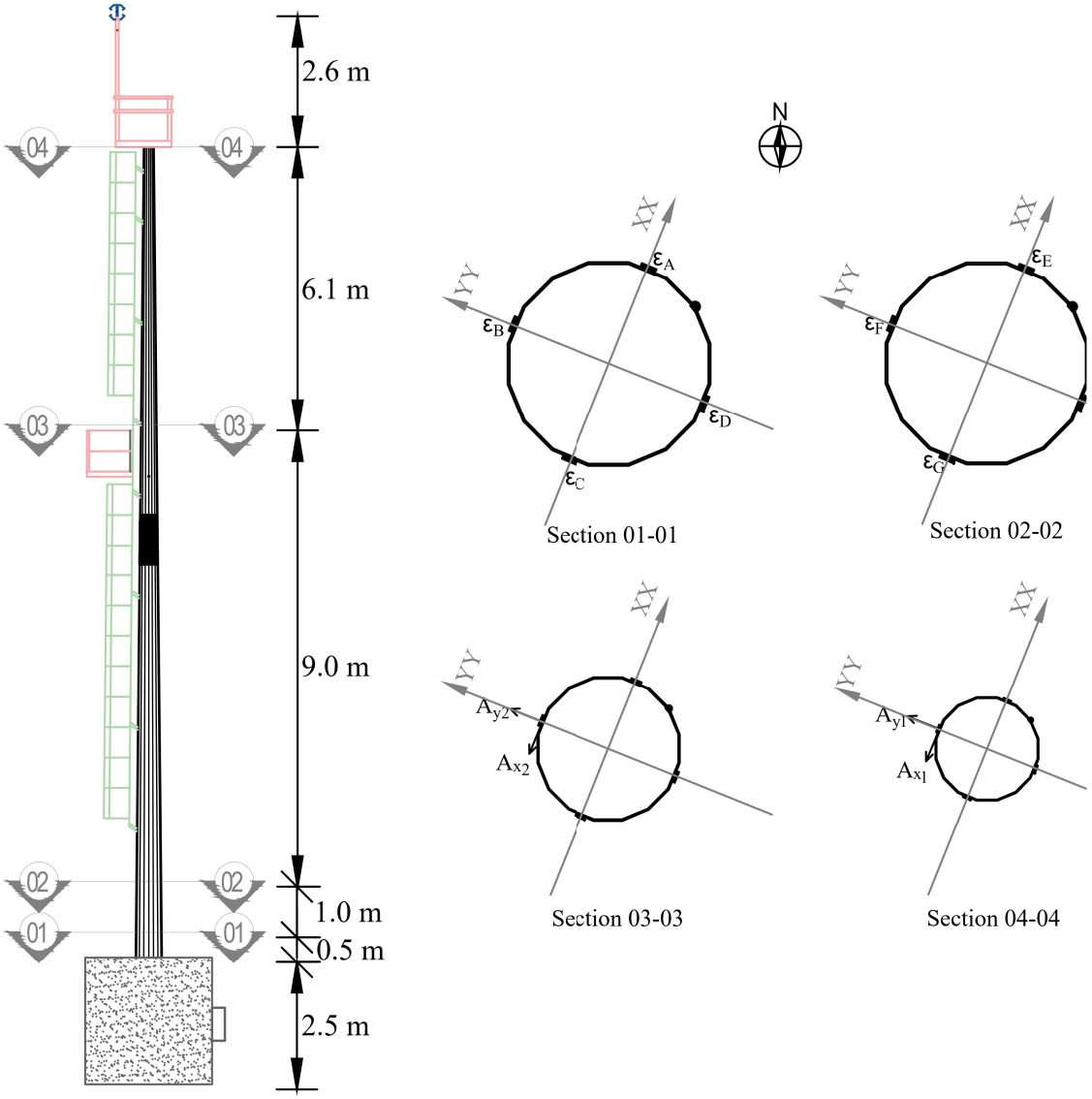

Fig. 2.2 Location of accelerometers and strain gauges on the monitored pole

- Location and direction of measurement sensors: The location of accelerometers at the top and 2/3rd of the height of the pole enabled the investigation of the first two mode shapes in the two principal directions which are single and double curvature bending respectively. Their position was selected to be at the anti-nodes of the first and second bending modes estimated from a numerical modal analysis. The provision of strain gauges on four points at each of the two heights and their orientation enabled strain registration due to bending along two perpendicular axes. The provision of a tri-axial accelerometer enabled the registration of acceleration in three perpendicular axes. This was important

for the calculation of displacement from strain gauges and acceleration. The provision of strain gauges towards the bottom of the pole where the bending stress will be high and the provision of accelerometers towards the top of the structure where the acceleration will be high was also a good approach to register signals with high amplitude to noise ratio. The location of the anemometer at the top of the tower avoided shedding or blockage effect from the monitored structure.

- Redundancy of sensors: Although two strain gauges on the faces of the cross-section along two perpendicular axes would have been adequate to measure the strain due to bending along the two perpendicular axes, the provision of four strain gauges at each of the two heights enabled a redundant system for noise compensation. In addition, the provision of four strain gauges at two levels also enabled redundancy of measurement in case the strain gauges at one of the heights fail.

- Selection of sensors: The selected strain gauge was a half-bridge system that compensate for temperature influences on the strain gauge. In addition, both the strain gauges and accelerometers were sensitive enough to pick up the expected signals of acceleration and strain measurement of the structure.

- The sampling frequency of sensors: The sampling frequency defines the upper limit of the frequency band that can be used for the analysis of the recorded signals. In this case, the sampling frequencies of the strain gauges, accelerometers, and anemometer were high enough to capture all the frequencies of interest.

- Synchronization of registered data: Synchronization of data from different sensors was not a problem because wired sensors with a single data acquisition system were used.

- Backup for power interruption: The data acquisition system is equipped with an uninterruptible power supply (UPS) as a backup in case a power interruption occurs.

Apart from the best practices summarized above, there are also points of improvement that should be considered for future wind and structural response monitoring systems.

- The monitoring system exported consecutive 6 hrs of registered wind-and-structural-response data in a text file which is later converted to a Matlab file during post-processing. However, a user interface that displays the measured data and summaries of the previously archived recordings should be considered for long-term monitoring systems as it facilitates the visualization and extraction of data. The user interface might also be useful to have a notification system during malfunctioning of the monitoring system.

- Although the monitored structure was provided with anemometers, the provision of meteorological sensors such as temperature, pressure, and humidity sensors could assist in the separation of high-intensity wind events into different types such as synoptic and thunderstorms.
- The provision of an anemometer at different heights will be useful to obtain information on the vertical profile of the wind speed. Although it might not be convenient to install several anemometers on the monitored tower, nearby towers can be considered.

2.3 Dynamic properties

Modal frequency, modal shape, and damping ratio are some of the parameters that dictate the dynamic response of any structure. Thus, estimating these parameters was the first important step in interpreting the registered response of the monitored structure.

Forced vibration test and operational modal analysis (OMA) are the two widely applied methods that are used to obtain the dynamic properties of structures. In recent years, operational modal analysis methods had major use in dynamic characterization because they do not require the mechanical vibration of the structure using external sources of excitation. The OMA methods use the registered response of the structure in ambient conditions to obtain the necessary dynamic properties. In this study, OMA methods such as the classical frequency domain approach, random decrement signature technique, and frequency domain decomposition method are used.

In the following sections, the commonly used OMA methods applied in this research are introduced, the selection of ambient vibration data for the application of the OMA methods is described, and finally, the dynamic properties are investigated.

2.3.1 Methods of dynamic identification

Classical frequency domain approach

This method is the most straightforward method for the identification of dynamic properties. It relies on the spectral density (SD) plot of the registered response of the structure under ambient conditions. The SD can be found through different approaches but the most common one is the Welch method (Welch, 1967). Applying the Welch method, the SD is obtained by calculating the Fourier transform of various segments of the response time history followed by the calculation of the ensemble average of the absolute amplitude squared of the Fourier-transformed segments. Once the SD is obtained, it is plotted as a function of frequency. If appropriate measurement

sensors are installed at proper locations of the structure for the ambient vibration registration, the peaks on the SD plot correspond to the modal frequencies of the structure. For example, the SD of strain or acceleration registration in the X and Y directions are expected to have resonant peaks at all modal frequencies associated with movement (translation or rotation) in the X and Y directions respectively. The number of vibration modes that can be identified through this method depends on the frequency of measurement of the sensors and the amplitude-to-noise ratio of the registered response. The accuracy of this method depends on the frequency resolution and the number of segments that are used to calculate the SD of the response.

If the modal frequencies are not very close to each other, a general idea of the modal shape can also be obtained from the SD plot by comparing the magnitude of the peaks of the response SD at various heights of the structure.

Structural damping associated with each vibration mode can also be obtained from the SD of response by measuring the bandwidth of the half-power point, which is the width of the SD at half of the peak value for each vibration mode. Equating the measured bandwidth with $2\xi n$, the damping ratio, ξ, for each vibration modal frequency, n, can be obtained. However, a more accurate measure of the damping ratio can be obtained by other methods that extract the part of the SD in the neighborhood of the modal frequencies and apply curve fitting procedures to either the SD or the correlation function of the SD. These more accurate methods and their applications are explained more clearly in Section 2.3.5.

Random decrement signature method

This method was proposed by Henry A. Cole in 1973 for failure detection and damping measurement in aerospace structures (Cole, 1973). It is based on the concept of random decrement signature (RDS). RDS is a curve obtained by calculating the ensemble average of segments of the response time history that are extracted based on a selected criterion of initial conditions. The procedure of estimation of RDS from a time history of response is illustrated in Fig. 2.3. In the example shown in Fig. 2.3, the segments are extracted based on the criteria that their initial amplitude is X_P and their slope $\dot{X}_P$ is zero. Thus segments of a predefined length satisfying the two criteria are extracted from the time history of vibration. The ensemble average of all the extracted segments will give the random decrement signature. The random decrement signature is mathematically expressed as follows (Kijewski and Kareem, 2000; Vandiver et al., 1982).

$$D_{X_P}(\tau) = E\left[X(t_2)|C\right] \tag{2.1}$$

where the expression on the right is the expected value of $X(t_2)$ given the initial condition at t_1 is satisfied. This initial condition, C, can be the following.

$$C = \begin{cases} X(t_1) = X_P & \\ X(t_1) = X_P & \cap \quad \dot{X}(t_1) = 0 \\ X(t_1) = 0 & \cap \quad \dot{X}(t_1) > 0 \end{cases}$$

The basis behind RDS is that averaging different segments of a response time history with predefined segment length and specific initial conditions will eliminate the random part of the response and results in the RDS which can be considered as directly proportional to the free vibration decay of the structure with an initial displacement. A mathematical justification for the RDS method was given by Vandiver et al. (1982) where it was concluded that for a linear time-invariant system excited by a stationary zero mean, Gaussian random process, the RDS is directly proportional to the autocorrelation function of the response. In addition, it was proved that for single degree of freedom (SDOF) systems excited by white noise, the autocorrelation function is exactly proportional to the free vibration decay of a structure with an initial displacement (Vandiver et al., 1982).

The free vibration decay curve of a single degree of freedom system, $X(t)$ is given by:

$$X(t) = \left[X(0)\cos\omega_D t + \left(\frac{\dot{X}(0) + X(0)\xi\omega}{\omega_D} \right) \sin\omega_D t \right] exp(-\xi\omega t) \tag{2.2}$$

where $\omega_D = \omega\sqrt{1-\xi^2}$; ω is the circular frequency; and ξ is the damping ratio of the system.

The envelope of the free vibration curve is given by $X(t) = E \cdot exp(-\xi\omega t)$, where E is a constant.

Once found, the RDS can be used to obtain the damping of the system through curve fitting. First, the RDS should be normalized to have a maximum amplitude of 1. Then depending on the initial condition for the RDS, different curve-fitting requirements can be applied. If the segments of time histories in the RDS were obtained using the initial condition of $\dot{X}(t_1) = 0$, both the damping and natural frequency of the system can be found by fitting Eq. 2.2 with $X(0) = 1$ and $\dot{X}(0) = 0$ to the RDS. Otherwise, the damping ratio can be found by fitting $X(t) = exp(-\xi\omega t)$ to the envelope of the RDS provided that the modal frequency is known.

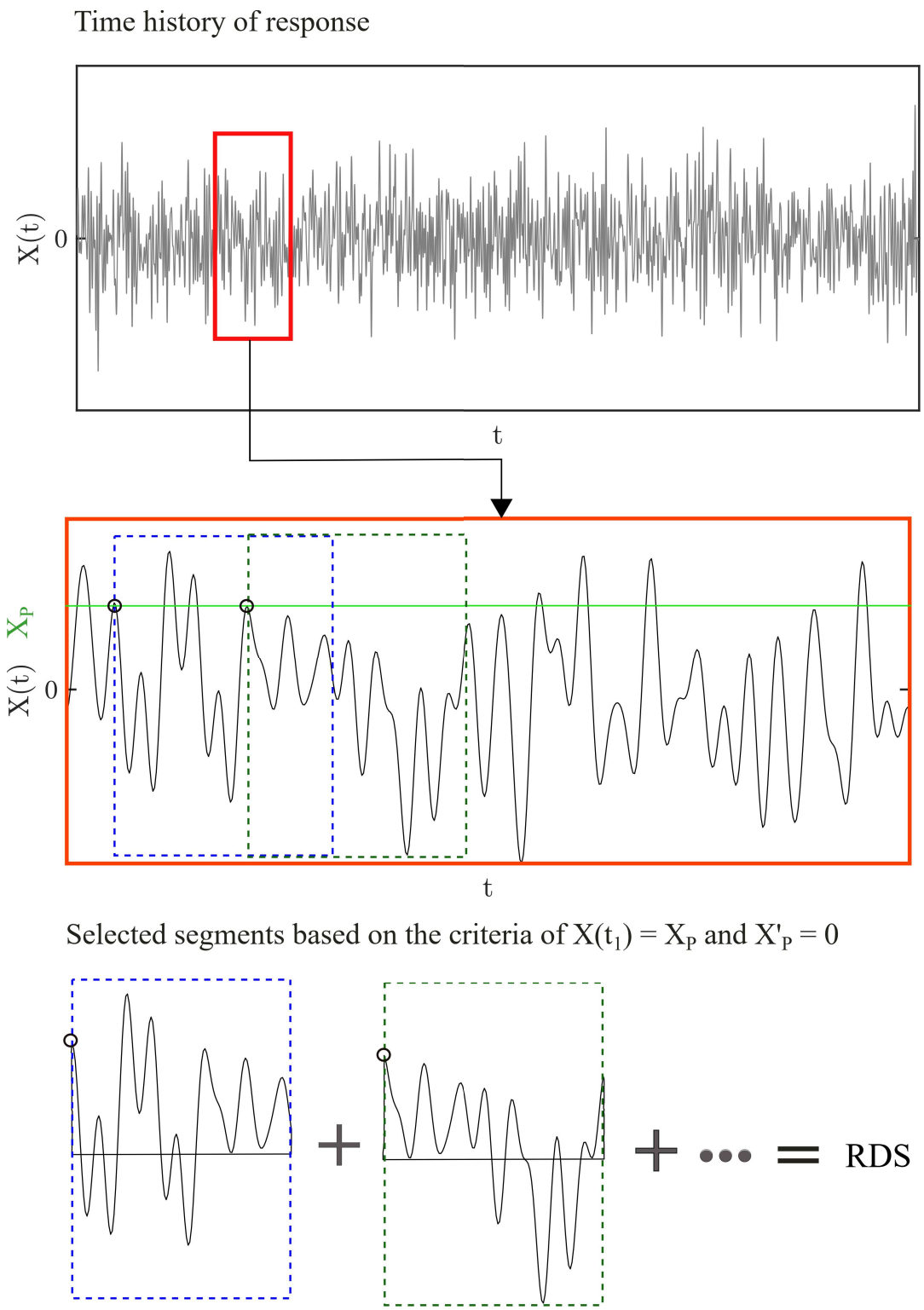

Fig. 2.3 Illustration of random decrement signature estimation

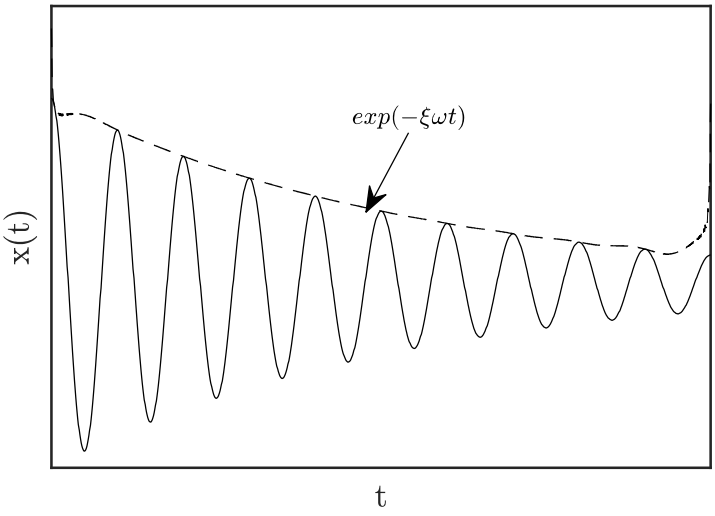

Fig. 2.4 Free decay of an SDOF with zero initial velocity

Frequency domain decomposition

Frequency domain decomposition (FDD) is a method introduced by Brincker et al. (2000). Its application is based on the spectral density matrix of the response of the structure measured by different channels at various heights of the structure. It is based on the following definition of the spectral density matrix of the response $\mathbf{G}_y(f)$

$$\mathbf{G}_y(f) = \mathbf{A}\mathbf{G}_q(f)\mathbf{A}^T \tag{2.3}$$

where $\mathbf{A}$ is the mode shape matrix $\mathbf{A} = [\mathbf{a}_1, \mathbf{a}_2, \ldots]$ and $\mathbf{G}_q(f)$ is the SD matrix of the modal coordinates.

If we now assume that the modal coordinates are uncorrelated, the SD matrix $\mathbf{G}_q(f)$ of the modal coordinates will be both diagonal and positive valued. Further, since we know that the SD matrix is Hermitian and that some complexity might be present in the mode shapes, we need to use Hermitian instead of the transpose. Thus, Eq. 2.3 becomes

$$\mathbf{G}_y(f) = \mathbf{A}[g_n^2(f)]\mathbf{A}^H \tag{2.4}$$

where $g_n^2(f)$ are the auto spectral densities (diagonal elements) of $\mathbf{G}_q(f)$.

If the response (vibration) time history of a structure measured by various channels is available, the SD matrix can be calculated using various methods. Then, the calculated SD

matrix, $\mathbf{G}_y(f)$, can be decomposed using singular value decomposition to have the form of Eq. 2.3 which for a complex, Hermitian, and positive definite matrix, takes the form

$$\mathbf{G}_y(f) = \mathbf{USU}^H = \mathbf{U}[s_n^2(f)]\mathbf{U}^H \tag{2.5}$$

It follows directly that the singular values $s_n^2(f)$ in the diagonal matrix $\mathbf{S}$ should be interpreted as the auto spectral densities of the modal coordinates, and the singular vectors - that is the columns in $\mathbf{U} = [u_1, u_2, \ldots]$ - should be interpreted as the mode shapes. By plotting the singular vectors as a function of frequency, the modal frequencies can be found by peak-picking. The singular vectors corresponding to the modal frequencies are interpreted as modal shapes. In addition, by extracting the part of the singular vector plot in the proximity of each modal frequency which is called "the spectral bell" in literature, damping ratios associated with each mode can be obtained.

2.3.2 Selection of data for system identification

All the dynamic identification methods introduced in the previous section are developed on the assumption that the structure is excited by a stationary and zero-mean input. Thus, initially, periods in which the structure was subjected to approximately stationary excitation have to be found. The reverse arrangement test is one of the methods for checking the stationarity of random processes (Bendat and Piersol, 2010). Thus, the stationarity of consecutive 1-hr wind speed data was checked using the reverse arrangement test. From the available 4230-hr data, a total of 84 segments of 1-hr wind speed data were found to satisfy the stationarity criteria with a confidence level of 95%.

As explained in Section 2.2, the structural response has been registered with accelerometers and strain gauges. Both of these registered responses can be used for dynamic system identification but in comparison, acceleration registrations were found to be easier to be used as they do not require pre-processing as in the case of strain registrations (explained in Chapter 3 Section 3.3.3). Thus, acceleration registrations were selected to be used for the dynamic system identification.

To further inspect the 84 segments of 1-hr data, plots of wind speed, wind direction, registered acceleration, and SD of registered acceleration were made for each of the segments. For example, Fig. 2.5 shows the wind speed, V, wind direction, α, acceleration registrations, and SD of accelerations for one of the 1-hr segments out of the 84. Similar plots like Fig. 2.5 were prepared for all 84 segments and by visually inspecting the acceleration registration and its SD, it was observed that the accelerometers at the top of the pole, A_{x1} and A_{y1}, were not working properly

in most of the 1-hr segments. From the visual inspection, the accelerometers at both heights were found to be working in 14 out of 84 1-hr segments. On the other hand, the accelerometers at 2/3 of the height of the pole, A_{x2} and A_{y2}, were working in all of the selected segments. Although the accelerometers at the top of the tower might have a better amplitude-to-noise ratio, the accelerometers at 2/3 of the height of the pole are also adequate for most of the system identification. Fig. 2.6 summarizes the mean wind speed of the 84 1-hr segments selected for the system identification and their occurrence in time. Black markers indicate segments where all accelerometers were working and blue markers indicate segments where only the accelerometers at 2/3 of the height of the pole are working. It can be observed that all the stationary segments selected for dynamic identification have a mean wind speed of lower than 10 m/s. This limits the scope of the damping ratio estimation because there are only a few data segments during significant wind intensity for the investigation of the aerodynamic damping.

2.3.3 Modal frequencies

The modal frequencies of the monitored structure were found through the classical frequency domain approach. Initially, SD was calculated for the 84 1-hr acceleration registrations, A_{x2} and A_{y2}, selected in Section 2.3.2 using the Welch method with segments of 2^{15} and 50 % overlap.

Fig. 2.7 shows an example of the SD of accelerations, A_{x2} and A_{y2}, plotted using one of the 1-hr time histories. Note that the two accelerometers register acceleration in orthogonal horizontal directions. Since the frequency of acceleration registration is 200 Hz, the cutoff frequency is 100 Hz. However, the axis of frequency in the SD plot is limited to 5 Hz for ease of peak identification. As explained in Section 2.3.1, the frequencies at the resonant peaks are identified as the modal frequencies. From Fig. 2.7, it can be observed that the first and second modes are very close to each other at a frequency of 0.75 Hz and 0.85 Hz, while the rest of the modal frequencies are above 3 Hz. For the application in this research, only the first two modes are considered to be significant (investigated in Chapter 3). Thus, the focus of subsequent sections will be only on the first two modes.

Long-term variability of the first two modal frequencies was studied by selecting 59 stationary time histories that had a mean 1-hr wind speed greater than 1 m/s out of the 84 1-hr time histories. The threshold on the mean wind speed was imposed to make sure that the amplitude-to-noise ratio is adequate for the resonant peak identification. The mean values of the first and second mode frequencies were found to be 0.75 and 0.85 Hz with a coefficient of variation of 1.05% and 1.24% respectively. Fig. 2.8 shows the first two modal frequencies and their variability with time and wind speed. It is evident that there is a slight variability with time probably because

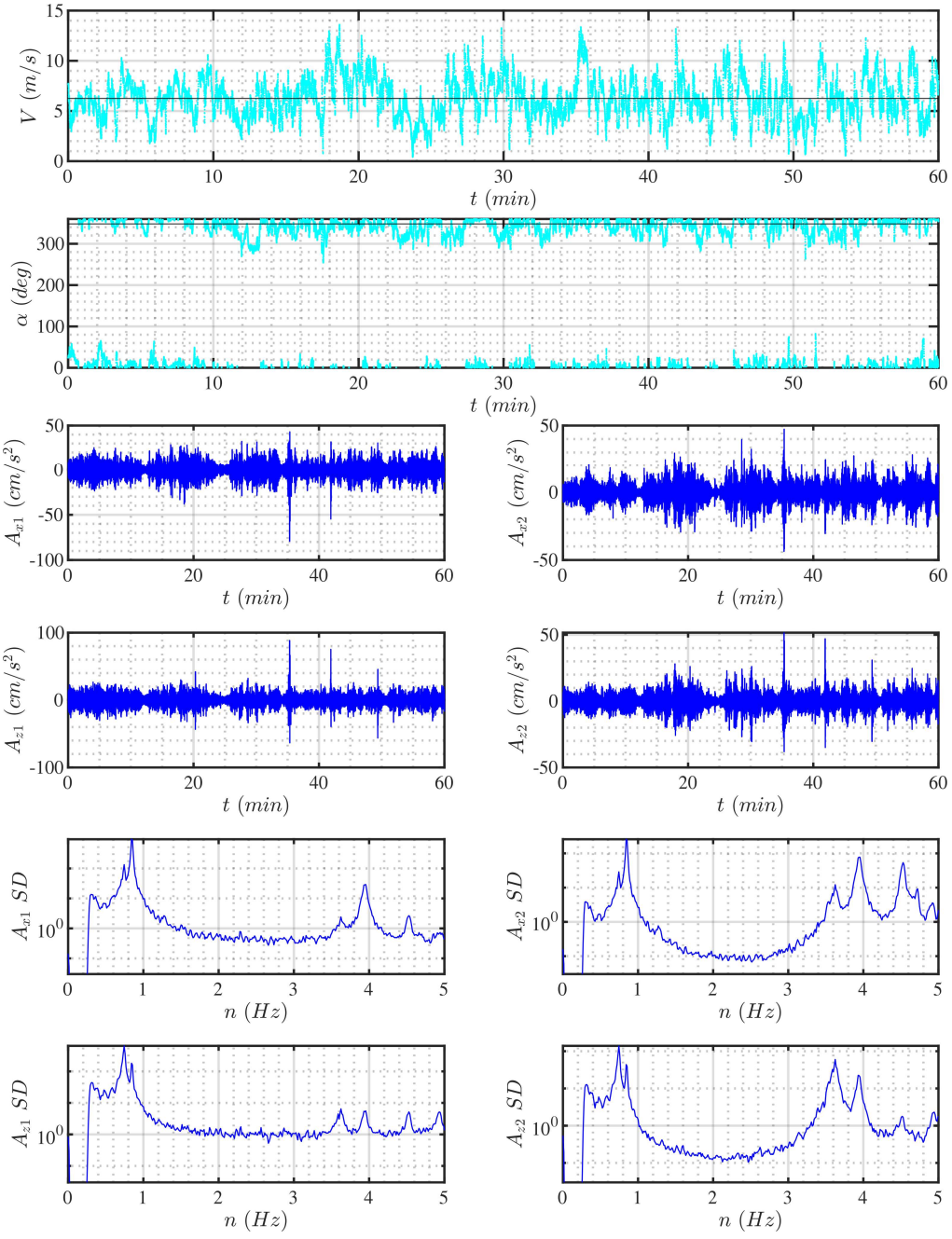

Fig. 2.5 Registered data for visual inspection

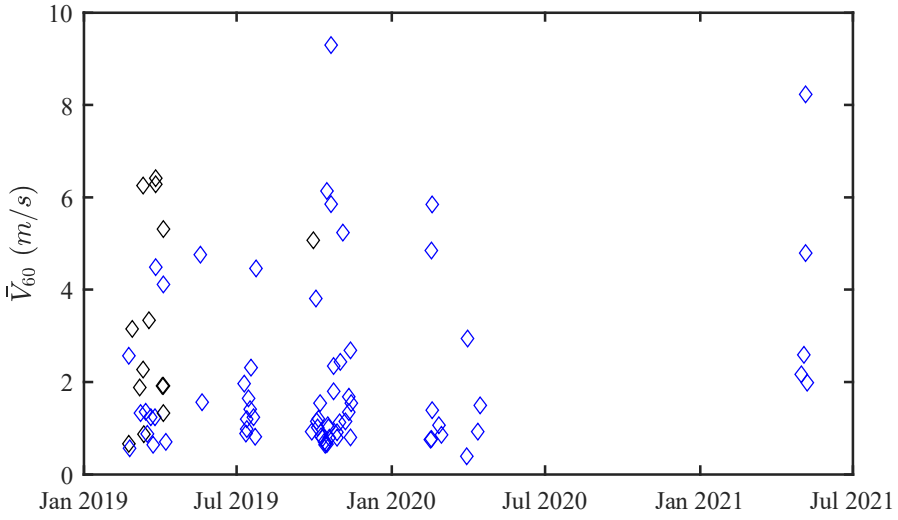

Fig. 2.6 Selected stationary data

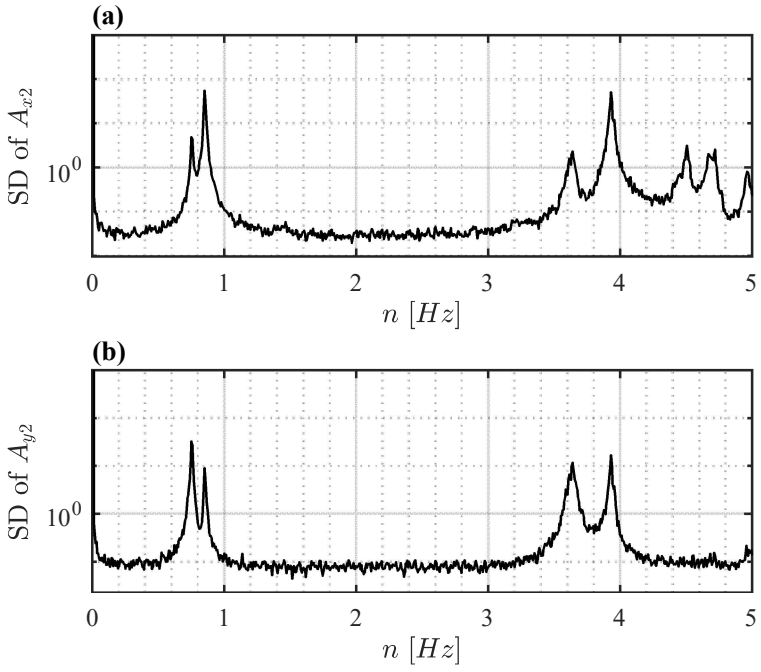

Fig. 2.7 SD of acceleration measurement

of a change in the lighting fixture at the top of the tower. However, an increasing or decreasing trend of modal frequencies with wind speed can not be observed from the plot.

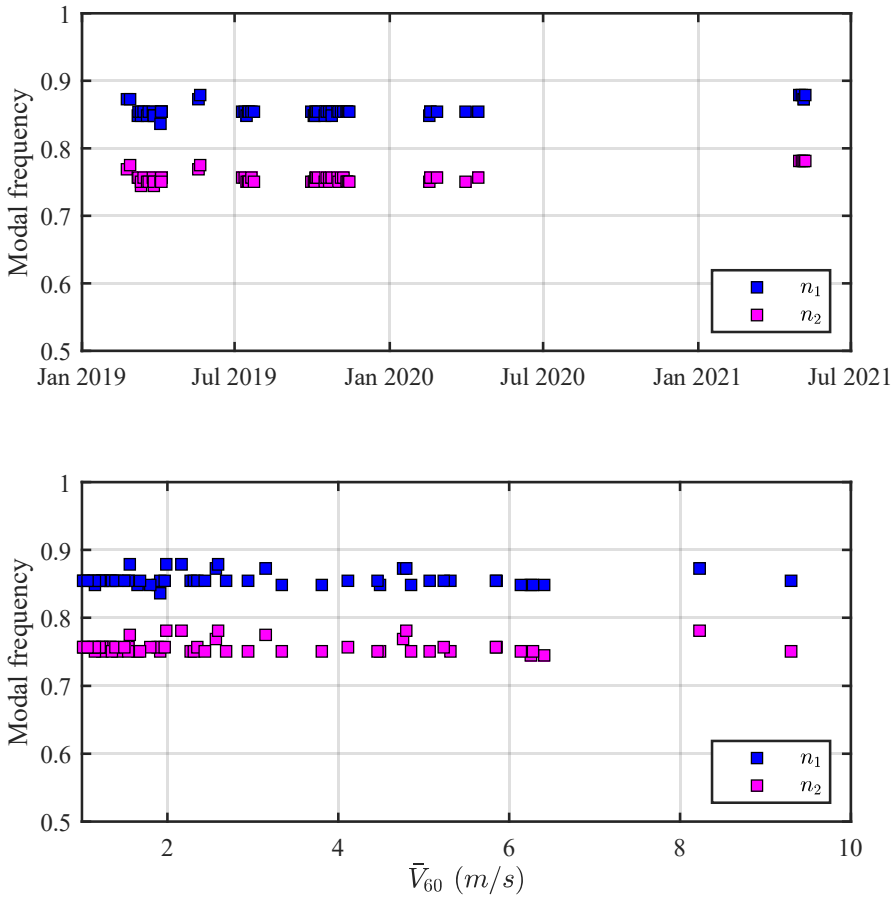

Fig. 2.8 The first two modal frequencies

Although the SD of the response was adequate to obtain the modal frequencies, the modal shapes and the axis of bending for each of the modal frequencies can not be easily identified from this plot. However, careful observation of the SD of responses that are orthogonal to each other can give some indication. For the monitored structure, the possibility of having torsional vibration mode as the first or second mode can be ruled out because the cross-section has high torsional stiffness. Comparing the SD plot of orthogonal response components such as A_{x2} versus A_{y2} in Fig. 2.7, the presence of the resonant peaks at 0.75 Hz and 0.85 Hz on both plots indicates that the first two modes are not bending modes along the axis of measurements of A_{x2} and A_{y2}. Investigating the axis of bending for each of the two modes is important because the pole is not

polar symmetric due to the presence of a ladder and an intermediate platform attached to one of the sides of the structure.

To obtain the axis of bending for each of the vibration modes, a trial and error procedure was applied by calculation of acceleration on assumed axes of bending and plotting the PSD. The assumed axes were rotated until the PSD of the strain calculated on the assumed axes showed only a single peak at either 0.75 Hz or 0.85 Hz. The acceleration registrations at 10.5 m above the base, A_{x2} and A_{y2}, were used and a procedure explained in Table 2.1 was applied to find the axes of bending corresponding to the first and second modes.

Table 2.1 Procedure for bending axis determination.

Step	Operation
1	Assume the axis of bending corresponding to the first two modes, axes X-Y, to be an axis rotated by an angle γ from the measurement axes, XX-YY. (Fig. 2.9)
2	Project the registered accelerations along XX-YY, A_{x2} and A_{y2}, to the new axes X-Y to get A'_{x2} and A'_{y2}.
3	Plot the SD of A'_{x2} and A'_{y2}
4	Check whether only one or both resonant peaks at 0.75 Hz and 0.85 Hz are present in the SD plots of A'_{x2} and A'_{y2}.
5	If only one of the resonant peaks at either 0.75 Hz or 0.85 Hz can be spotted in the SD plots of A'_{x2} and A'_{y2}, the assumed value of γ is corresponding to the axis of bending for the first and second bending modes (Eg. See Fig. 2.10 (c) and (d)). If not (Eg. See Fig. 2.10 (a) and (b)), repeat Steps 2 to 4 changing the value of γ until this condition is satisfied.

Following this procedure, the axes of bending of the structure corresponding to the 1^{st} and 2^{nd} modes of vibrations were found to be an orthogonal set of axes, that are rotated by $\theta = 23.5^{o}$ (Fig. 2.9) clockwise from the local reference system of response measurement, XX-YY. The 1^{st} mode of bending was found to be along the Y axis at 0.75 Hz and the 2^{nd} mode of bending was found to be along the X axis at 0.85 Hz (Fig. 2.9). In subsequent sections, we will refer to the axes of bending of the first and second bending modes, X-Y, as the principal axes of bending of the structure. Since the first two modes are single curvature bending about axes orthogonal to each other, we will refer to these modes as the first bending modes in the principal directions with frequencies, $n_{X,1}$ and $n_{Y,1}$.

2.3.4 Modal shapes

Mode shapes for the first bending modes in the principal directions were estimated by applying the frequency domain decomposition (FDD) method (Brincker et al., 2001; Brincker and Zhang,

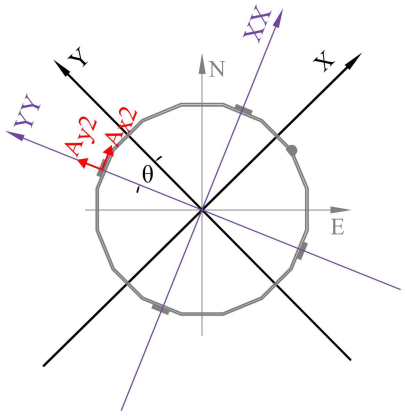

Fig. 2.9 Orientation of the principal axes with respect to the local reference system

2009; Tamura et al., 2002; Zhang et al., 2005). First, 1-hr acceleration data in which both accelerometers were working are selected (Section 2.3.2). Then, the acceleration registrations in the orthogonal directions, XX-YY, were projected along the principal bending axes, X-Y.

$$\begin{aligned} A_{Xj} &= A_{xj}\cos(\theta) + A_{yj}\sin(\theta) \\ A_{Yj} &= A_{yj}\cos(\theta) - A_{xj}\sin(\theta) \end{aligned} \tag{2.6}$$

where $j = 1,2$; and $\theta = 23.5°$.

Then, according to the FDD technique, the power spectral density (SD) matrix was calculated for the response in the X direction using zero acceleration at the bottom, A_{X2} at 10.5 m, and A_{X1} at the top of the structure. Similarly, the SD matrix was calculated for the response in the Y direction using zero acceleration at the bottom, A_{Y2} at 10.5 m, and A_{Y1} at the top. The SD was calculated using a segment length of 2^{15} points with 50% overlap. The calculated SD matrices were decomposed through the singular value decomposition technique to have the modal shape matrices and a diagonal matrix of singular values at each frequency. The modal shape vectors corresponding to modal frequencies $n_{1,Y} = 0.75\ Hz$ and $n_{1,X} = 0.85\ Hz$ were identified as the modal shape vectors $\psi_{Y,1}$ and $\psi_{X,1}$ respectively. The Mode shapes vectors indicated that the first modes in the principal directions are single curvature bending. The modal shapes in the X and Y directions were mathematically modeled through a power function $(z/H)^{\zeta_{i,1}}$, where z is the height above the base, H is the total height of the structure, $\zeta_{i,1}$ is a constant and $i = X,Y$. The constant $\zeta_{i,1}$ was found for both principal directions using the modal shape vectors $\psi_{Y,1}$ and $\psi_{X,1}$. The investigation for modal shape was done for 14 1-hr time histories of accelerations selected in Section 2.3.2 to check variability in the estimation of modal shape. As a result, the

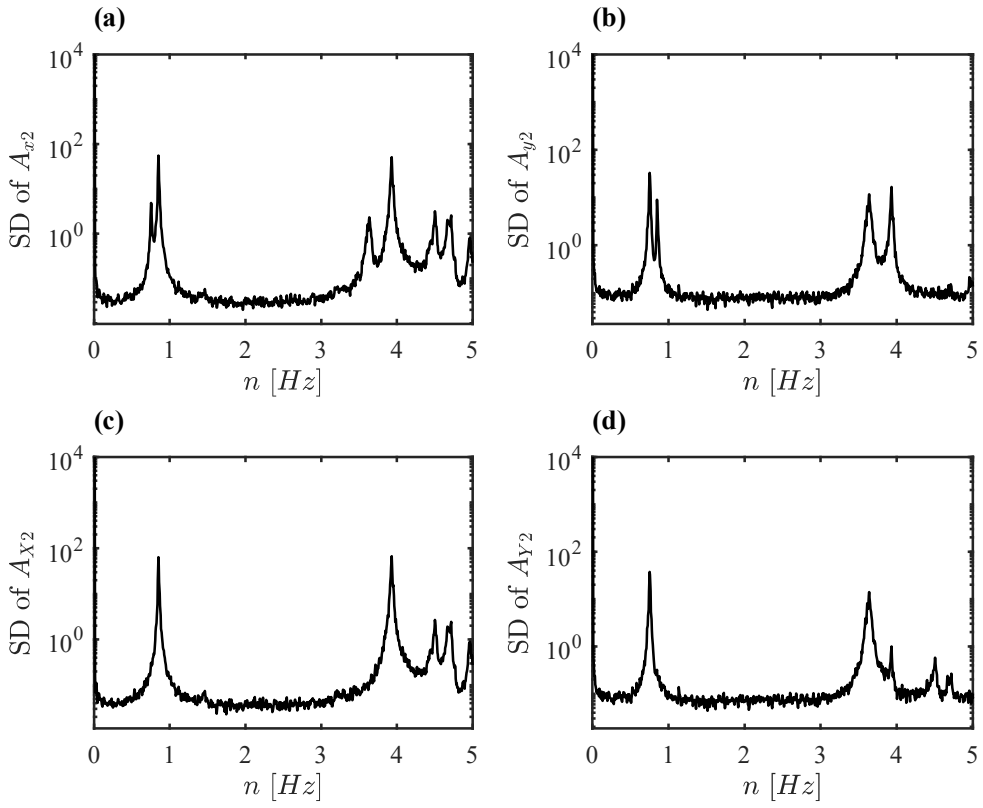

Fig. 2.10 SD of registered acceleration ((a) and (b)) and acceleration along the principal axes ((c) and (d))

mean value of the power coefficients was found to be $\zeta_{X,1} = 1.6$ and $\zeta_{Y,1} = 1.9$, with a coefficient of variation of 2.3% and 1.6% respectively.

2.3.5 Damping ratio

The damping ratio of the monitored structure was investigated using the random decrement signature method and classical frequency domain approaches.

Random decrement signature method

The random decrement method was applied using acceleration registrations of the identified 84 1-hr time histories (Section 2.3.2). Because the accelerometer at the top of the structure was not working properly during most of the stationary signals, only acceleration registrations at the

height of 10.5 m, A_{x2} and A_{y2}, were used. Initially, the registered accelerations along the local axis of measurements, XX-YY, were projected on the principal axis of the structure, X-Y, to get A_{X2} and A_{Y2} (Eq. 2.6).

The two acceleration registrations, A_{Y2} and A_{X2}, were bandpass filtered to extract responses corresponding to the 1^{st} mode vibrations in the two principal directions Y and X respectively. A_{X2} was bandpass filtered between 0.8 and 0.9 Hz, while A_{Y2} was bandpass filtered between 0.7 and 0.8 Hz. The random decrement signature (RDS) was calculated by extracting 40 seconds segments, that satisfy the criteria of initial amplitude, $X(t_2) = X_P$. In this case, since acceleration measurement was used to obtain the random decrement signature, the initial condition will be defined as $A(t_2) = A_P$. However, to maximize the number of segments extracted from the 1-hr time history and thereby increase the accuracy of the RDS, a threshold of amplitude was applied instead of a single value. Segments within the 3% threshold of A_P were also considered as satisfying the initial condition. To increase the probability of obtaining higher numbers of segments from the 1-hr time history, 8 values, ranging from 10% to 80% of the maximum response amplitude were selected to be the initial condition A_P. Using these criteria, RDS was calculated for each of the 84 1-hr time histories. Thus, a total of $84 \times 8 = 672$ RDS were calculated in each principal direction.

After the RDS were calculated, they were normalized to have a maximum amplitude of 1. Then, the normalized envelope of an SDOF free vibration decay, $X(t) = exp(-\xi\omega t)$ was fitted to the envelope of the RDS through the nonlinear least square method to obtain the damping ratio. $X(t) = exp(-\xi\omega t)$ with $\omega = 2\pi(0.75)$ was fitted to the envelope of RDS obtained using A_{Y2} and $X(t) = exp(-\xi\omega t)$ with $\omega = 2\pi(0.85)$ was fitted to the envelop of RDS obtained using A_{X2}. Fig. 2.11 shows an example plot of the RDS with its envelope as well as the plot of the frequency decay (FD) and its envelope obtained through curve fitting for a single case out of the 672.

The goodness of fit for each of the 672 RDS was also calculated through the R-squared (Coefficient of determination) value. Then, from the 8 results obtained for each of the 84-time histories, the result corresponding to the maximum R-squared value was selected. Thus, a single damping ratio was obtained for each of the 84-time histories. Finally, results that have an R-squared value of less than 99% were disregarded. This process was automated using a MatLab script and the process yielded 19 results for damping in the X direction and 11 results for damping in the Y direction. The damping ratio corresponding to the first mode bending in the Y direction, $\xi_{Y,1}$, was found to be 0.42% with a coefficient of variation of 26%. The damping ratio corresponding to the first mode bending in the X direction, $\xi_{X,1}$, was found to be 0.4% with a coefficient of variation of 21%. The number of 40-second segments used for the calculation of the RDS was between 160 and 4366. Fig. 2.12 shows the damping ratios, $\xi_{X,1}$ and $\xi_{Y,1}$, calculated

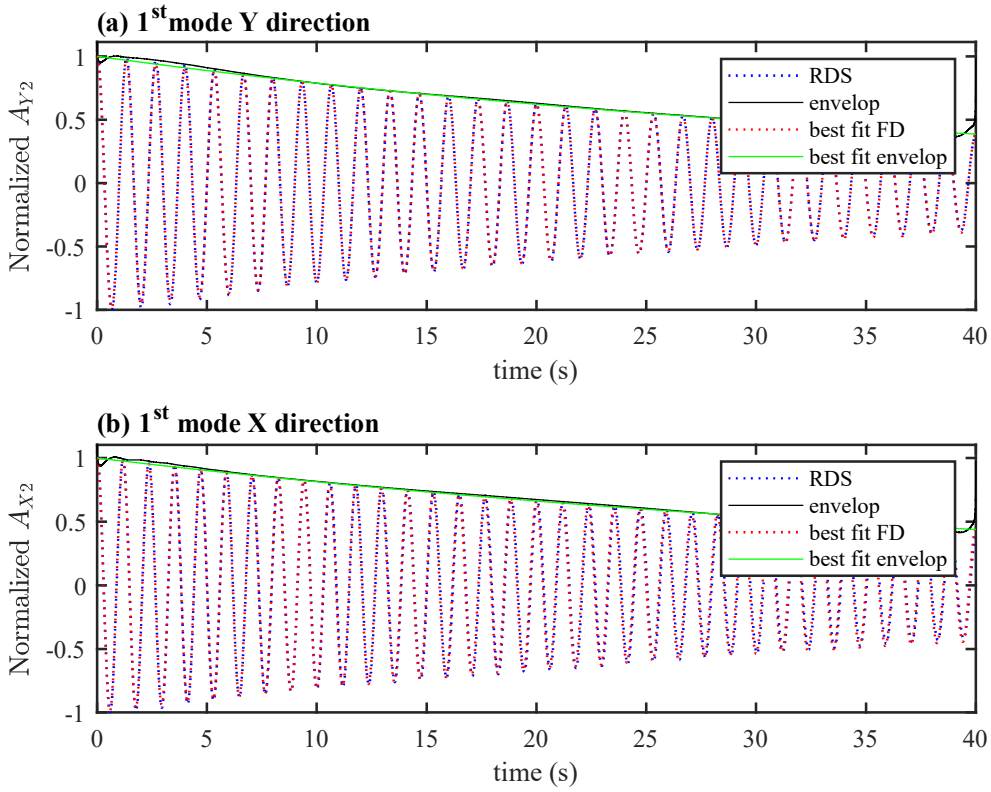

Fig. 2.11 Example of RDT method application

using the random decrement signature technique. The calculated damping ratios are plotted, as a function of the mean wind speeds, $\bar{V}_{60}$, of the 1-hr segments used for the estimation of the damping values (Fig. 2.12(a)), as a function of the time period of the 1-hr segments used for the estimation of the damping values (Fig. 2.12(b)), as a function of the amplitude of accelerations that were used as the initial condition A_P for extracting the 40-second segments (Fig. 2.12(c)), and as a function of the number of 40-second segments that were ensemble averaged to obtain the random decrement signature for the calculation each of the damping ratios (Fig. 2.12(d)). From visual observation, there is no clear indication of a relationship between the estimated damping ratios and the considered parameters. However, it should be noted that most of the 1-hr data segments used for the damping estimation are vibrations of the structure during a low-intensity wind (less than 10 m/s), and in addition, the estimated damping ratios were filtered based on the goodness of fit between the RDS and the free vibration decay of an SDOF system.

In general, considering the high uncertainty of damping estimation usually highlighted in the literature, it can be stated that the proper selection of stationary inputs coupled with the

application of criteria of goodness of fit in the damping estimation using the random decrement signature applied in this research yielded a satisfactory result of damping ratio with comparably low variability.

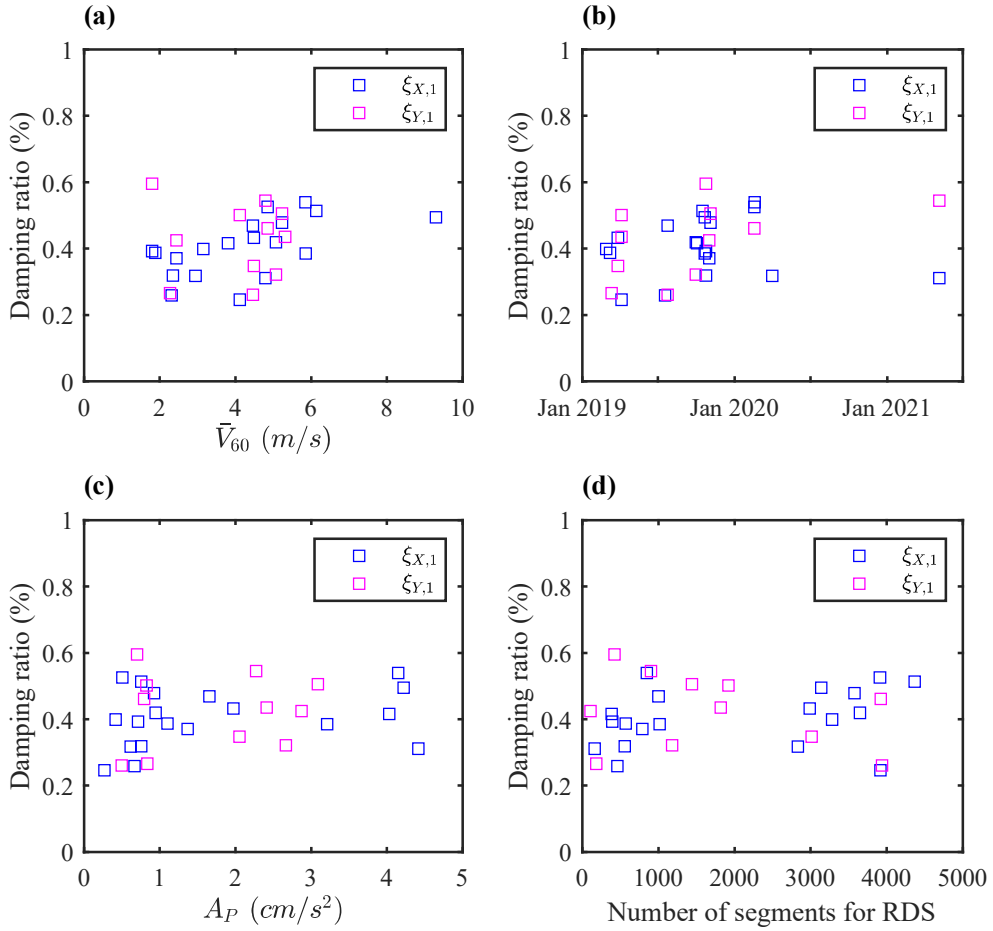

Fig. 2.12 Damping ratio obtained using RDS method

Classic frequency domain approach

The damping ratio of the monitored structure was calculated following classic frequency domain approaches that use the auto spectral density of acceleration registration as the main input. Initially, the acceleration registrations in the orthogonal directions, A_{x2} and A_{y2}, were projected along the principal axes X - Y and A_{X2} and A_{Y2} were found. Then the auto spectral density was calculated using the Welch method with a segment length of 2^{16} points and 50% overlap. Since the frequency of acceleration measurement is 200 Hz, the resolution frequency of the SD was

$\approx 305 \times 10^{-3}$ Hz. The part of the SD around the modal frequencies $n_{X,1} = 0.85$ and $n_{Y,1} = 0.75$ was extracted from the SD of A_{X2} and A_{Y2} respectively. The extracted segment of SD is referred to as 'the spectral bell' in literature because of its bell shape. Fig. 2.13 illustrates the spectral bell (in red) and the parent SD. There is no clearly defined limit for the upper and lower bound frequencies of the spectral bell in the literature although some recommend $\pm 1Hz$ from the modal frequency. However, Brincker et al. (2001) suggested the use of modal assurance criteria (MAC) to ensure that the extracted spectral bell corresponds to only the modal frequency of interest and that contributions of other modes are not mixed.

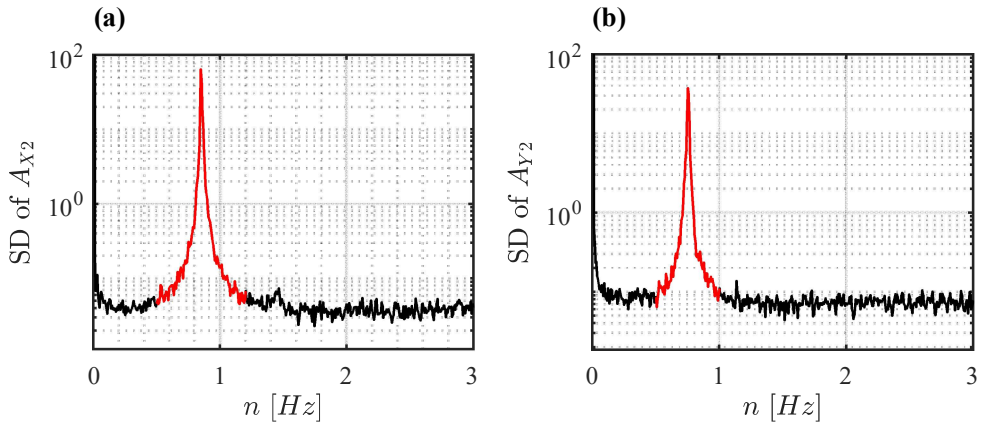

Fig. 2.13 Extraction of the spectral bell from the SD

By looking at the SD of acceleration, a threshold in the range of 0.05 - 0.35 Hz was considered to be sufficient to extract the spectral bell. The spectral bells such as shown in red in Fig. 2.13 were extracted by considering a threshold of 0.35 Hz for the upper and lower frequency band. This means that the bandpass frequencies were modal frequencies $\pm 0.35Hz$.

A separate check was made to make sure that the bandpass thresholds for the extraction of the spectral bell were not too wide to mix frequency contents of higher modes. This was done by calculating the modal shape vector corresponding to every frequency through the FDD method as explained in previous sections and calculating the MAC value for the lower and upper bound frequencies. This was implemented through the use of acceleration measurements at the two heights of the structure. The MAC number calculated at the lower and upper bound frequency was greater than 99%. Thus, the upper and lower bound frequencies were considered adequate.

Once the spectral bell is extracted, two methods were applied to get the damping ratio. These methods will be referred to as method 1 and method 2 in the subsequent discussions.

In method 1, first, stationary zero mean acceleration time history was generated from the spectral bell using Monte Carlo simulation. Then, the normalized-unbiased autocorrelation function for the generated time history was calculated. Finally, the damping ratio was obtained

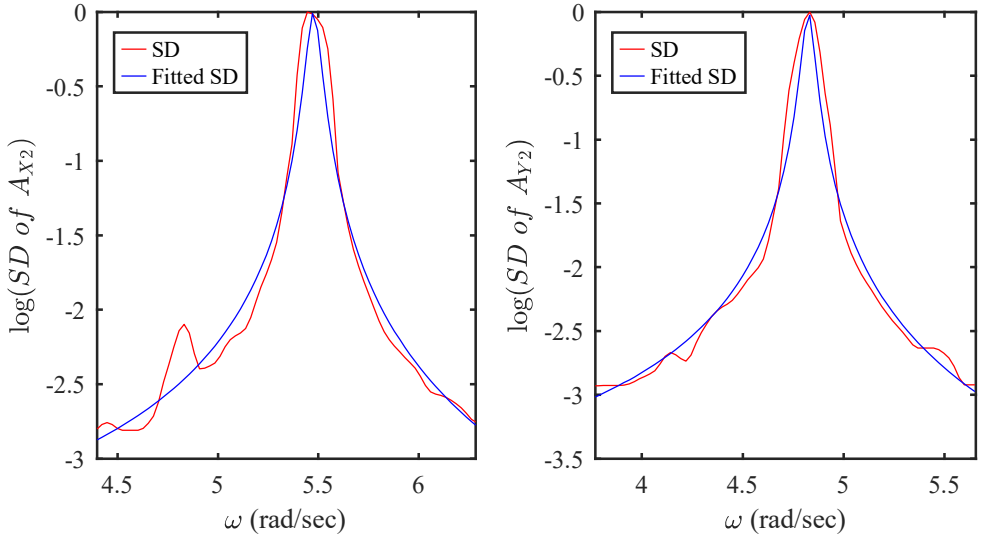

Fig. 2.14 Example of curve fitting of the FRF squared on the spectral bell

by fitting the envelope of the free decay of an SDOF, $exp(-2\xi\omega)$, to the envelope of the autocorrelation function.

Method 2 is based on the assumption that the excitation is white noise and thus the spectral bell is proportional to the square of the frequency response function (FRF) of an SDOF (Carassale and Percivale, 2008; Pagnini et al., 2018). The FRF squared of an SDOF is given by

$$|H(\omega)|^2 = \frac{1}{m^2\omega_0^4}\frac{1}{\left(1-\frac{\omega^2}{\omega_0^2}\right)^2+4\xi^2\frac{\omega^2}{\omega_0^2}} \tag{2.7}$$

The normalized FRF squared has a maximum magnitude of 1 and is given by

$$|H(\omega)|^2 = \frac{4\xi^2}{\left(1-\frac{\omega^2}{\omega_0^2}\right)^2+4\xi^2\frac{\omega^2}{\omega_0^2}} \tag{2.8}$$

Thus, the normalized FRF squared was fitted to the normalized spectral bell through the nonlinear least square method to find the modal frequency and damping. The fitting was done in the logarithmic representation to enhance its efficiency as recommended in Carassale and Percivale (2008). Fig. 2.14 shows the fitting between the normalized FRF squared and the normalized spectral bell for one of the considered time histories.

These two methods have been applied to the 84-time histories selected in Section 2.3.2 to calculate damping ratio. The results are further filtered by removing results in which the goodness of the fit measured in terms of R-squared value for method 1 was less than 95%. This way, 26 and 22-time histories were found to satisfy the R-squared threshold value for damping ratios, $\xi_{X,1}$ and $\xi_{Y,1}$ respectively. The results are summarized in Table 2.2.

Considering the high uncertainty of damping ratio estimation using OMA methods in the literature, the variability of the calculated damping ratio with a maximum coefficient of variation of less than 35% can be regarded as satisfactory and this could be attributed to the selection of approximately stationary vibration records and the application of criteria of goodness of fit in the damping estimation.

Figs. 2.15 and 2.16 show the variability of the estimated damping ratio with respect to the mean wind speed, the period, and the R-squared value of the fit. In all cases, a clear correlation and an increasing or a decreasing trend are not evident.

Table 2.2 Damping estimation using classic frequency domain approaches

Method	$\xi_{1,X}$		$\xi_{1,Y}$	
	mean [%]	cov [%]	mean [%]	cov [%]
1	0.55	34.8	0.59	29.6
2	0.58	30.4	0.63	27.1

Due to the availability of 1-hr acceleration data sampled at a frequency of 200 Hz, the damping ratio of the monitored structure was estimated using the classic frequency domain approach considering a segment length of 2^{16}. However, segment lengths of 2^{13}, 2^{14}, and 2^{15} were also considered to see if there is variability in damping estimation depending on the frequency resolution of the SD. Fig. 2.17 shows the variability of the mean damping ratio depending on the number of data points (segment length) considered for the SD. It can be observed that the damping ratio decreases as the frequency resolution increases. The decrease in damping ratio with the frequency resolution has a gentle slope after the segment length of 2^{15}. This finding is in agreement with the Tamura et al. (2002) in which damping is shown to reduce as the number of data points increases. Thus, it should be highlighted that a sufficiently long vibration record is very important to estimate the damping ratio through SD-based methods.

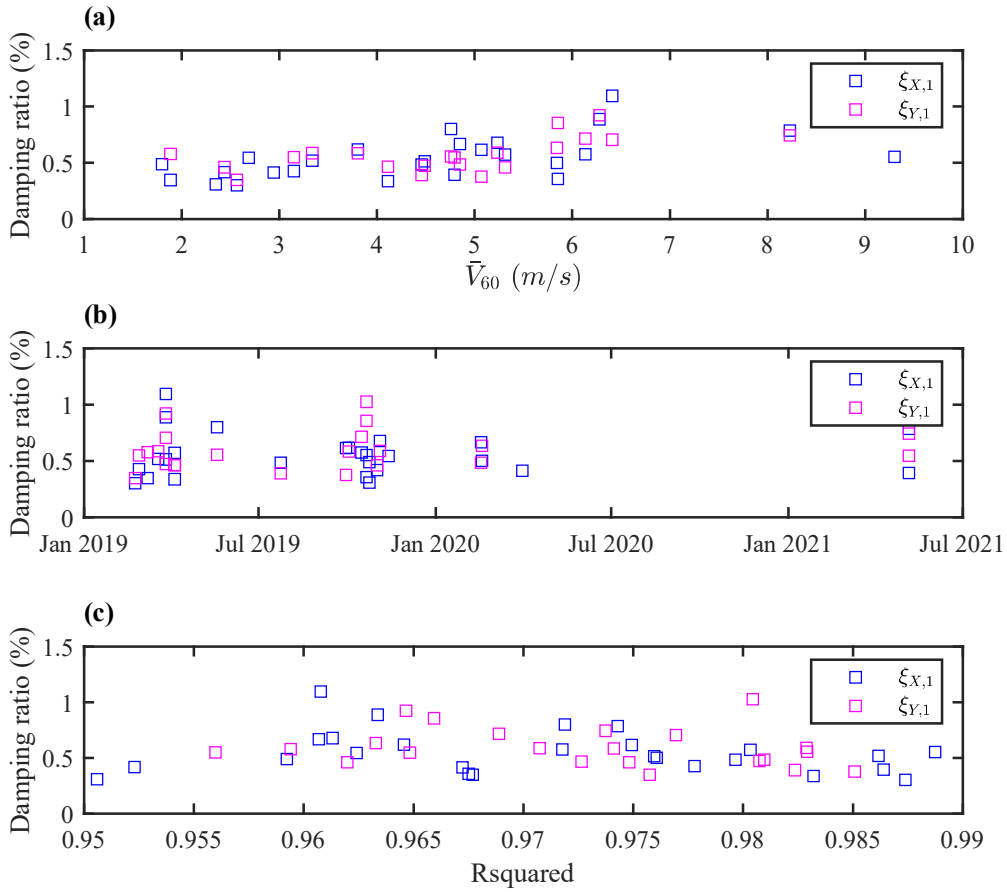

Fig. 2.15 Damping ratio obtained using classic frequency domain approach: Method 1

2.4 Aerodynamic properties

An investigation of the aerodynamic properties of the monitored structure was previously carried out by Andrea Orlando (Orlando et al., 2023) in the Giovanni Solari boundary layer wind tunnel at the University of Genova (https://www.gs-windyn.it/wind-tunnel/). Although the aerodynamic properties evaluation was not part of this thesis, the results of the experiments by Orlando et al. (2023) are reported here for the sake of completeness.

Three scaled models have been realized. A 3D model of the top platform, 1:5 scale, reproduces all the equipment at the top of the tower: the metallic frame, the spotlights, and the security camera (Fig. 2.18a). Two sectional 1:8 scale models, realized by 3D printing (Fig. 2.19a),

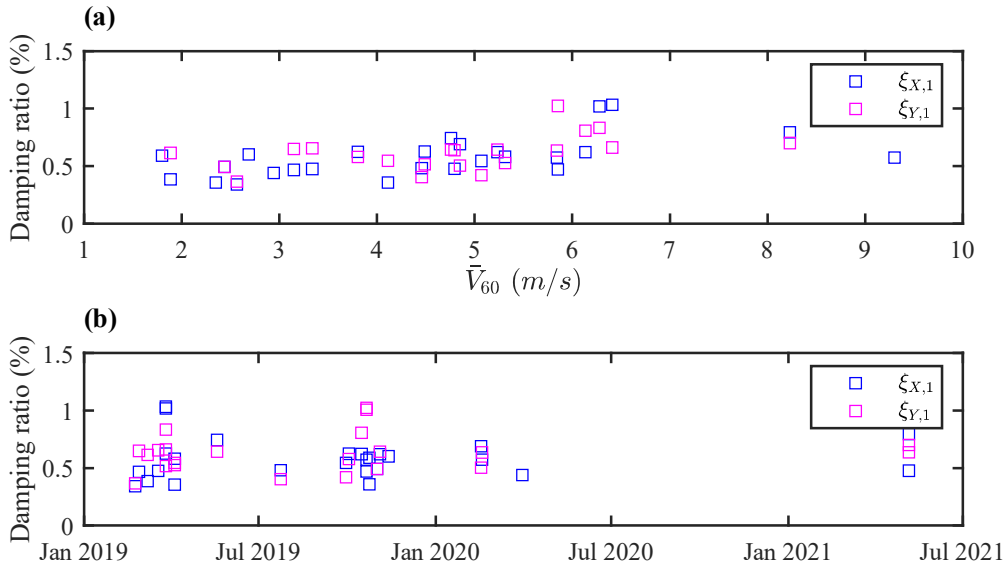

Fig. 2.16 Damping ratio obtained using classic frequency domain approach: Method 2

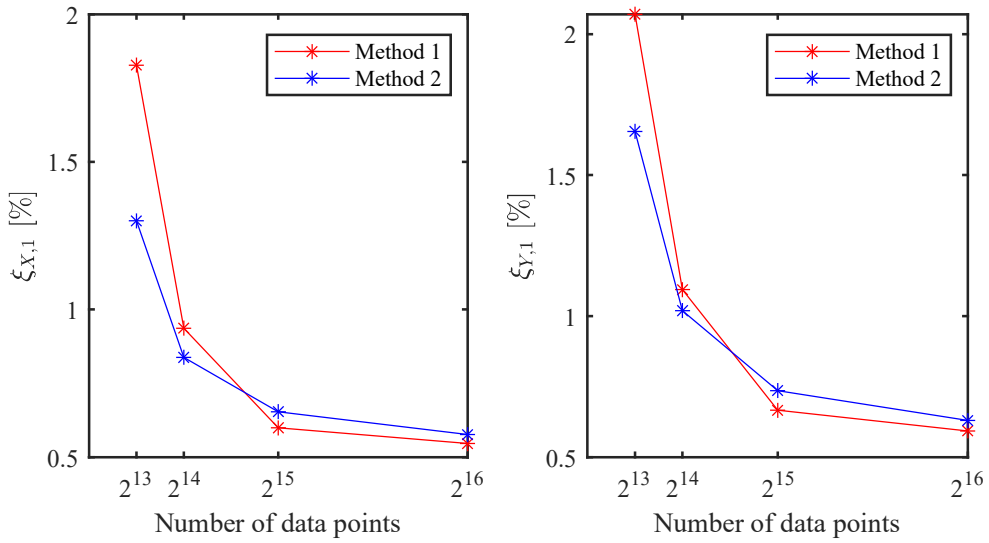

Fig. 2.17 Variation of damping ratio with data points of SD

represent the top and bottom segments of the tapered shaft, which has a 16-sided polygonal cross-section. They also reproduce the rounded corners, the weld, and the external ladder.

Models have been subjected to static tests to measure mean force coefficients and Strouhal number varying angle of attack, flow velocity, and turbulence intensity. The mean force coefficients of the models have been evaluated as:

$$C_i = \frac{\bar{F}_i}{\frac{1}{2}\rho \bar{u}^2 A_{ref}} \qquad i = d, l \tag{2.9}$$

where $\bar{u}$ is the reference mean wind velocity (time average of the pitot measure); A_{ref} is the reference area of the models; ρ is the air density; $\bar{F}_d$ and $\bar{F}_l$; are the time average of the aerodynamic force acting in the longitudinal and lateral directions respectively.

The mean force coefficients of the sectional models used for this work are reported in Figs. 2.18b and 2.19b. They have been obtained in turbulent flow ($I_u = 7.5\%$) with $\bar{u} = 11.0$ m/s. Further details of the description of the experiment and results can be found in Orlando et al. (2023)

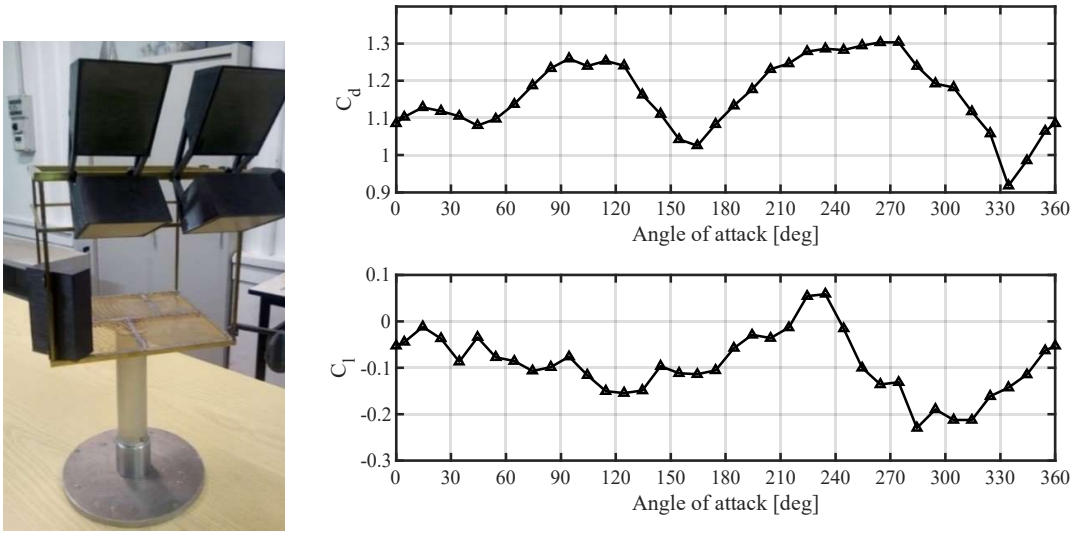

(a) (b)

Fig. 2.18 3D top platform model (a) and relevant mean force and moment coefficients as a function of angle of attack (b). $\bar{u} = 11.0 m/s$.

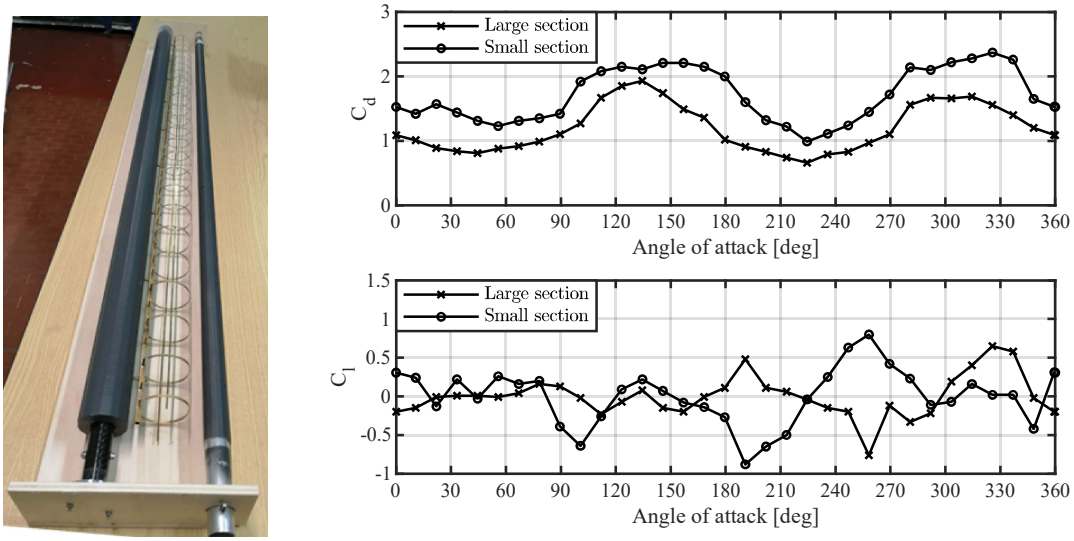

(a) (b)

Fig. 2.19 Sectional models (a) and relevant mean force coefficients as a function of angle of attack (b). Turbulence intensity $I_u = 7.5\%$; $\bar{u} = 11.0 m/s$.

2.5 Conclusion

- The dynamic properties of the monitored structure such as the modal frequency, modal shape, and damping ratio were estimated using operational modal analysis methods.
- The availability of long-term vibration data added to the novelty of the research in the selection of proper stationary inputs of vibration during the ambient conditions and in the study of the variability of the estimated dynamic properties with important parameters such as wind speed, the goodness of fit, . . . , etc.
- The first mode frequencies in the two principal directions were found using the power spectral plot with a minimal uncertainty quantified by a coefficient of variation value of less than 1.25%.
- The mode shape of the first modes in the two principal directions was estimated using the frequency domain decomposition technique. A very small variability quantified by a coefficient of variation value of less than 2.3% was observed.
- The proper selection of stationary inputs coupled with the application of criteria of goodness of fit in the damping estimation using the random decrement signature applied in this research yielded a satisfactory result of damping ratio with comparably low variability.

- The results of the calculated damping ratio through the classic frequency domain approaches were also satisfactory in terms of variability and this could be attributed to the selection of approximately stationary vibration records, the use of a high-resolution spectral density curve, and the application of criteria of goodness of fit in the damping estimation.

- The application of classic frequency domain approaches for the estimation of the damping ratio is found to be highly dependent on the frequency resolution of the power spectral density curve. This highlights the importance of using sufficiently long vibration data and high-resolution PSD for the proper estimation of the damping ratio.

- Estimation of the dynamic properties of the structure, especially the damping ratio, during transient events, was not possible because the operational modal analysis techniques are developed on the assumption the ambient vibration is due to a stationary input. This limited the scope of the system identification and the prevalence of aerodynamic damping during transient events could not be investigated. Future studies might consider the contribution of aerodynamic damping in short-lived transient events such as downbursts in comparison to ABL events.

References

Bashor, R., Bobby, S., Kijewski-Correa, T., and Kareem, A. (2012). Full-scale performance evaluation of tall buildings under wind. *J. Wind Eng. Ind. Aerodyn.*, 104-106:88–97.

Bendat, J. S. and Piersol, A. G. (2010). *Random Data*, volume 82. John wiley and sons, Inc., Publication, 4th editio edition.

Brincker, R. ., Zhang, L. ., and Andersen, P. (2000). Output-Only Modal Analysis by Frequency Domain Decomposition. In *Proc. ISMA25*, pages 717–723.

Brincker, R. and Ventura, C. (2015). *Introduction to operational modal analysis*, volume 6. John Wiley and Sons Ltd.

Brincker, R., Ventura, C. E., and Andersen, P. (2001). Damping Estimation by Frequency Domain Decomposition. In *Proc. IMAC 19*, pages 698–703.

Brincker, R. and Zhang, L. (2009). Frequency Domain Decomposition Revisited. In *Proc. 3rd Int. Oper. Modal Anal. Conf.*, volume 2, pages 615–626.

Carassale, L. and Percivale, F. (2008). Modal identification of wind-Excited slender structures by acceleration and strain measurements. In *7th Eur. Conf. Struct. Dyn. EURODYN 2008*, Southampton.

Cole, H. A. (1973). On-Line Failure Detection and Damping Measurement of Aerospace Structures By Random Decrement Signatures. Technical report.

Dagliesh, W. A. and Rainer, J. H. (1978). Measurements of wind induced displacements and accelerations of a 57 storey building in Toronto, Canada. In *Proc. 3Rd Colloq. Ind. Aerodyn. Build. Aerodyn. Aachen, Fed. Rep. Ger. Jun 14-16, 1978, C.*, volume 2, pages 67–78.

Dalgliesh, W. (1982). Comparison of model and full-scale tests of the Commerce Court Building in Toronto. In *Proc. Int. Work. Wind Tunn. Model. Criteria Tech. Civ. Eng. Appl. Gaithersburg, Maryland, April 1982*, pages 575–589.

Fu, J. Y., Wu, J. R., Xu, A., Li, Q. S., and Xiao, Y. Q. (2012). Full-scale measurements of wind effects on Guangzhou West Tower. *Eng. Struct.*, 35:120–139.

Hudson, D., Keightley, W., and Nielsen, N. (1964). A new method for the measurment of the natural periods of buildings. *Bull. Seismol. Soc. Am.*, 54(1):233–241.

Jeary, A. P., Miere, and Ellis, B. R. (1983). On predicting the response of tall buildings to wind excitation. *J. Wind Eng. Ind. Aerodyn.*, 13(1-3):173–182.

Kijewski, T. and Kareem, A. (2000). Reliability of Random Decrement Technique For Estimates of Structural Damping. In *8th ASCE Spec. Conf. Probabilistic Mech. Struct. Reliab.*, number 1, pages 1–6.

Kijewski-Correa, T., Kilpatrick, J., Kareem, A., Kwon, D.-K., Bashor, R., Kochly, M., Young, B. S., Abdelrazaq, A., Galsworthy, J., Isyumov, N., Morrish, D., Sinn, R. C., and Baker, W. F. (2006). Validating Wind-Induced Response of Tall Buildings: Synopsis of the Chicago Full-Scale Monitoring Program. *J. Struct. Eng.*, 132(10):1509–1523.

Kijewski-Correa, T. and Kochly, M. (2007). Monitoring the wind-induced response of tall buildings: GPS performance and the issue of multipath effects. *J. Wind Eng. Ind. Aerodyn.*, 95(9-11):1176–1198.

Kijewski-Correa, T. and Pirnia, J. D. (2007). Dynamic behavior of tall buildings under wind: Insights from full-scale monitoring. *Struct. Des. Tall Spec. Build.*, 16(4):471–486.

Li, Q. S., Fang, J. Q., Jeary, A. P., and Wong, C. K. (1998). Full scale measurements of wind effects on tall buildings. *J. Wind Eng. Ind. Aerodyn.*, 74-76:741–750.

Li, Q. S., Fu, J. Y., Xiao, Y. Q., Li, Z. N., Ni, Z. H., Xie, Z. N., and Gu, M. (2006). Wind tunnel and full-scale study of wind effects on China's tallest building. *Eng. Struct.*, 28(12):1745–1758.

Li, Q. S. and Wu, J. R. (2007). Time–frequency analysis of typhoon effects on a 79-storey tall building. *J. Wind Eng. Ind. Aerodyn.*, 95(12):1648–1666.

Li, Q. S., Wu, J. R., Liang, S. G., Xiao, Y. Q., and Wong, C. K. (2004). Full-scale measurements and numerical evaluation of wind-induced vibration of a 63-story reinforced concrete tall building. *Eng. Struct.*, 26(12):1779–1794.

Li, Q. S., Xiao, Y. Q., and Wong, C. K. (2005). Full-scale monitoring of typhoon effects on super tall buildings. *J. Fluids Struct.*, 20(5):697–717.

Li, Q. S., Xiao, Y. Q., Wong, C. K., and Jeary, A. P. (2003). Field measurements of wind effects on the tallest building in Hong Kong. *Struct. Des. Tall Build.*, 12(1):67–82.

Littler, J. and Ellis, B. (1992). Full-scale measurments to determine the response of Hume Point to wind loading. *J. Wind Eng. Ind. Aerodyn.*, 44:1085–1096.

Momomura, Y., Marukawa, H., Okamura, T., Hongo, E., and Ohkuma, T. (1997). Full-scale measurements of wind-induced vibration of a transmission line system in a mountainous area. *J. Wind Eng. Ind. Aerodyn.*, 72(1-3):241–252.

Ohkuma, T., Marukawa, H., Niihori, Y., and Kato, N. (1991). Full-scale measurement of wind pressures and response accelerations of a high-rise building. *J. Wind Eng. Ind. Aerodyn.*, 38(2-3):185–196.

Orlando, A., Pagnini, L., and Pia Repetto, M. (2023). Wind tunnel tests of a hexadecagonal cylinder with imperfections and ancillaries: aerodynamic characterization and technical discussion. *Eng. Struct.*, 274(March 2022):115114.

Pagnini, L., Piccardo, G., and Repetto, M. P. (2018). Full scale behavior of a small size vertical axis wind turbine. *Renew. Energy*, 127:41–55.

Tamura, Y., Zhang, L., Yoshida, A., Nakata, S., and Itoh, T. (2002). Ambient Vibration Tests and Modal Identification of Structures by FDD and 2DOF-RD Technique. In *Proc. Struct. Eng. world Congr.*, Yokohama,Japann.

Vandiver, J. K., Dunwoody, A. B., Campbell, R. B., and Cook, M. F. (1982). A Mathematical Basis for the Random Decrement Vibration Signature Analysis Technique. *J. Mech. Des.*, 104:307–313.

Wan, J. W., Li, Q. S., Han, X. L., and Xu, K. (2022). Investigation of structural responses and dynamic characteristics of a supertall building during Typhoon Kompasu. *J. Wind Eng. Ind. Aerodyn.*, 230.

Wang, Y. W. and Ni, Y. Q. (2022). Full-scale monitoring of wind effects on a supertall structure during six tropical cyclones. *J. Build. Eng.*, 45.

Ward, H. and Crawford, R. (1966). Wind-induced vibrations and building modes. *Bull. Seismol. Soc. Am.*, 56(4):793–813.

Welch, P. D. (1967). The Use of Fast Fourier Transform for the Estimation of Power Spectra: A Method Based on Time Averaging Over Short, Modified Periodograms. *IEEE Trans. Audio Electroacoust.*, 15(2):70–73.

Yang, B., Zhu, H., Wüchner, R., and Zhang, Q. (2021). Monitoring of wind effects on a wind-sensitive hybrid structure with single-layer cable-net curtain walls under Typhoon Muifa. *J. Build. Eng.*, 44.

Zhang, L., Brincker, R., and Andersen, P. (2005). An Overview of Operational Modal Analysis. In *Proc. 1st Int. Oper. Modal Anal. Conf.*, pages 179–190.